AIMS Mathematics, 10(11): 25667–25707.
DOI: 10.3934/math.20251137
Received: 12 June 2025
Revised: 09 September 2025
Accepted: 18 September 2025
Published: 06 November 2025

https://www.aimspress.com/journal/Math

Research article

Application of LAPM and ABM methods to a fractional SCIR model of pneumonia diseases

Muflih Alhazmi[1,*], **Safa M. Mirgani**[2], **Abdullah Alahmari**[3] **and Sayed Saber**[4,5]

[1] Mathematics Department, Faculty of Science, Northern Border University, Arar, Saudi Arabia
[2] Imam Mohammad Ibn Saud Islamic University (IMSIU), College of Science, Department of Mathematics and Statistics, Riyadh, Saudi Arabia
[3] Department of Mathematics, Faculty of Science, Umm Al-Qura University, Mecca, Saudi Arabia
[4] Department of Mathematics, Faculty of Science, Al-Baha University, Al-Baha, Saudi Arabia
[5] Department of Mathematics and Computer Science, Faculty of Science, Beni-Suef University, Beni-Suef, Egypt

* **Correspondence:** Email: Sayed011258@science.bsu.edu.eg; Tel: +9660597625063.

Abstract: We develop a fractional SCIR (susceptible-carrier-infected-recovered) model for pneumococcal pneumonia using Caputo derivatives of order $0 < \varrho \leq 1$ to capture memory effects from long carriage, waning immunity, and reinfection. The force of infection explicitly accounts for carriers' transmissibility. Using a next-generation approach, we derive the basic reproduction number $\mathscr{R}_0$ and prove the global asymptotic stability of the disease-free equilibrium when $\mathscr{R}_0 < 1$ and of the endemic equilibrium when $\mathscr{R}_0 > 1$ via Lyapunov functionals and a fractional LaSalle principle. Numerically, we combine the Laplace-Adomian-Padé method (LAPM) with a fractional Adams-Bashforth-Moulton scheme (ABM) to capture memory-driven transients. A sensitivity analysis identifies transmission intensity and routing into carriage as the dominant epidemic drivers, while treatment and mortality exert mitigating effects. A control extension yields a closed-form, control-adjusted $\mathscr{R}_0$; a minimal vaccination threshold; and an optimal control problem solved numerically. Finally, we outline a calibration workflow linking the model-predicted incidence to surveillance data, permitting a statistical estimation of the fractional order. Altogether, incorporating carriers and fractional memory modifies the thresholds and persistence conditions, producing dynamics that are more consistent with pneumococcal epidemiology.

Keywords: pneumococcal pneumonia; fractional-order model; stability analysis; nonlocal memory effects; numerical simulations; SCIR model
Mathematics Subject Classification: 34A08, 34L99, 92D30

1. Introduction

Pneumococcal pneumonia, caused by Streptococcus pneumoniae, remains a major global health challenge, disproportionately affecting young children, the elderly, and immunocompromised individuals. Despite advancements in antibiotics and vaccines, it continues to account for substantial morbidity and mortality worldwide. The transmission dynamics are complex, shaped by host immunity, bacterial virulence, and environmental conditions.

Over the years, several mathematical models have been developed to understand and control the spread of pneumococcal pneumonia. Ong'ala et al. [1] studied bacteremic pneumococcal pneumonia in children using bifurcation theory and equilibrium stability. Mochan et al. [2] proposed an ordinary differential equation-based model for host immune response in murine strains, while Drusano et al. [3] demonstrated the interaction of antibiotics and granulocyte-mediated bacterial killing. Ndelwa et al. [4] explored the effects of treatment and screening, whereas Kosasih et al. [5] applied wavelet-based cough sound analysis for rapid diagnosis. Other studies extended the scope to comorbidities and environmental links: César et al. [6] examined the association between particulate matter and pediatric pneumonia, Marchello et al. [7] conducted a meta-analysis of atypical pathogens, Cheng et al. [8] studied influenza-associated secondary pneumonia, and Kosasih and Abeyratne [9] highlighted diagnostic limitations in resource-limited regions. Tilahun et al. [10, 11] introduced cost-effective control and co-infection models with typhoid, while Raj et al. [12] and Kizito and Tumwiine [13] focused on cough-based disease classification and microbial interactions.

Further extensions incorporated complexities such as co-infections and delays. Mbabazi et al. [14] modeled influenza A and pneumococcal pneumonia co-infection, Tilahun [15] analyzed pneumonia-meningitis dynamics, and Diah and Aziz [16] proposed predictive stochastic frameworks. Additional contributions include Tilahun [17] on bacterial co-infections, Mbabazi et al. [18] on delay differential analysis, Otoo et al. [19] on vaccination models, and Zephaniah et al. [20] on graphical transmission representations. Fractional and fractal-fractional models have also emerged: Saber and Alahmari [21], Althubyani et al. [22, 23], and Naveed et al. [24] extended susceptible-carrier-infected-recovered (SCIR) frameworks with memory and delay dynamics.

Fractional-order modeling and optimal control continue to show strong performance across applied domains [25]. In epidemic systems with carrier states, global stability results on heterogeneous networks provide a rigorous foundation [26]. Beyond epidemiology, fractional models are widely applied in viscoelasticity [27], quantum dynamics [28], Liu systems [29], and biological systems such as diabetes [30–32]. They have also been applied to zoonotic [33], tobacco [34], influenza [35], and other apllications [36–40]. These studies confirm the versatility of fractional calculus for capturing memory and nonlocal effects in diverse scientific fields. Most classical epidemiological models are formulated using ODEs [2–4, 14, 15], which provide useful insights but neglect hereditary effects and long memory. Such features are crucial in pneumococcal epidemiology, where extended carriage, waning immunity, and reinfection strongly influence its dynamics. This limitation motivates the adoption of fractional-order models, which naturally incorporate memory. Recent works confirm that memory-driven and delay-dependent structures alter epidemic predictions, particularly during latent periods, quarantine, and social interventions [41–43]. In parallel, nonstandard finite difference (NSFD) methods preserve positivity and stability in discrete-time simulations, ensuring structural fidelity [44–46].

To solve fractional systems, a variety of analytical and numerical approaches have been proposed, including the Adomian decomposition method (ADM) [47], the Laplace-Adomian decomposition method (LADM) [48], the modified ADM [49], the multistep generalized differential transform method (MSGDTM) [50], the predictor-corrector Adams-Bashforth-Moulton (ABM) method [51], Galerkin finite elements [52], Legendre wavelets [53], and spectral collocation [54], see also [55–58]. In this work, we emphasize two complementary approaches: the Laplace-Adomian-Padé method (LAPM) and the ABM scheme. LAPM accelerates series expansions with Padé approximants, yielding accurate semi-analytical solutions, while ABM offers stable and efficient time-marching. Together, they balance accuracy and efficiency, enabling robust simulation and validation.

Motivated by these considerations, we propose a new fractional-order SCIR model for pneumococcal pneumonia, formulated using Caputo derivatives. Unlike prior fractional studies, which often considered only susceptible-infected-recovered (SIR) or susceptible-vaccinated-carrier-infected-recovered (SVCIR) structures, our framework explicitly incorporates the carrier class, which is epidemiologically central to pneumococcal transmission but is often overlooked. We derive the basic reproduction number, analyze the local and global stability, and perform a sensitivity analysis to identify the key transmission drivers. Numerical simulations using LAPM and ABM confirm the theoretical results and highlight the influence of fractional dynamics on disease persistence and control.

To connect the baseline SCIR dynamics to policy design, we augment the model in Section 7 with three time-dependent interventions, contact reduction $u_\delta(t) \in [0, 1)$, treatment enhancement $u_\tau(t) \geq 0$, and vaccination $v(t) \geq 0$, acting, respectively, on transmission, removal, and susceptibility. This modifies the force of infection to

$$\lambda(t) = \delta(1 - u_\delta(t))\frac{I(t)+\varpi C(t)}{N(t)}.$$

We prove the positivity and boundedness under controls and derive a closed-form, control-adjusted reproduction number $\mathscr{R}_0(u_\delta, u_\tau, v)$, together with an explicit minimal vaccination threshold $v_{\min}(u_\delta, u_\tau)$ ensuring $\mathscr{R}_{\text{eff}} < 1$, while emphasizing the role of carrier transmissibility ϖ in line with networked carrier models [57]. A quadratic-cost optimal control problem is then posed, characterized via Pontryagin's maximum principle, and solved numerically with a forward-backward sweep and the fractional ABM integrator. Simulations compare individual and combined interventions, quantify cost-effectiveness, and demonstrate how memory reshapes thresholds, peaks, and elimination time, consistent with recent advances in fractional optimal control [25].

The remainder of the paper is structured as follows. Section 2 reviews the mathematical preliminaries. Section 3 presents the baseline SCIR model. Section 4 establishes the well-posedness. Section 5 derives the threshold and global stability. Section 6 analyzes the sensitivity. Section 7 develops the optimal-control problem. Section 8 describes the numerical methods. Section 9 reports numerical experiments. Sections 10 and 11 provide some conclusions and future perspectives.

2. Fundamental concepts

A function $f(t)$, where $t > 0$, is said to belong to the space C_α for some $\alpha \in \mathbb{R}$ if it can be represented as $f(t) = t^p g(t)$ for some $p > \alpha$, where $g(t)$ remains continuous over $[0, \infty)$. Furthermore, the function

is said to be in the space C_α^m if its m^{th} derivative, $f^{(m)}$, belongs to C_α for some $m \in \mathbb{N}$ (see [59] for details).

Definition 2.1. *[59] The Riemann-Liouville fractional integral of order $\alpha > 0$ for a function $f \in C_\alpha$, with $a \geq 0$, is defined as*

$$_{RL}J_a^\alpha f(t) = \frac{1}{\Gamma(\alpha)} \int_a^t (t-\tau)^{\alpha-1} f(\tau)\, d\tau, \quad t > a,$$

where $\Gamma(\cdot)$ denotes the gamma function.

Definition 2.2. *[59] For a real number $\alpha > 0$, the Caputo fractional derivative of order α with $a \geq 0$ is defined via the Riemann-Liouville integral as*

$$_C\mathscr{D}_a^\alpha f(t) = {}_{RL}J_a^{m-\alpha} f^{(m)}(t),$$

Equivalently,

$$_C\mathscr{D}_a^\alpha f(t) = \frac{1}{\Gamma(m-\alpha)} \int_a^t \frac{f^{(m)}(\tau)}{(t-\tau)^{\alpha-m+1}}\, d\tau,$$

where $m-1 < \alpha < m$, $t \geq a$, and $f \in C_{-1}^m$ with $m \in \mathbb{N}$.

An important property linking the Riemann-Liouville fractional integral and the Caputo derivative of the same order α is given by [59]:

$$_{RL}J_a^\alpha {}_C\mathscr{D}_a^\alpha f(t) = f(t) - \sum_{k=0}^{m-1} f^{(k)}(a)\, \frac{(t-a)^k}{k!},$$

where $m-1 < \alpha < m$, and $f \in C_\alpha^m$.

Lemma 2.1. *[59] The Laplace transform of the Caputo fractional derivative of order $m-1 < \alpha < m$ is*

$$\mathscr{L}\left\{{}_C\mathscr{D}_a^\alpha f(t)\right\} = s^\alpha F(s) - \sum_{k=0}^{m-1} s^{\alpha-k-1} f^{(k)}(0),$$

where $F(s) = \mathscr{L}\{f(t)\}$.

Definition 2.3. *[59] For parameters $\alpha, \beta > 0$ and $z \in \mathbb{C}$, the Mittag-Leffler functions are defined as*

$$E_\alpha(z) = \sum_{j=0}^{\infty} \frac{z^j}{\Gamma(j\alpha+1)}, \qquad E_{\alpha,\beta}(z) = \sum_{j=0}^{\infty} \frac{z^j}{\Gamma(j\alpha+\beta)}.$$

Lemma 2.2. *[55] Let $u(t)$ be a function such that $\mathscr{D}_{0,t}^\varrho u(t)$ exists for all t. Then,*

$$\mathscr{D}_{0,t}^\varrho u(t) \leq -\Pi\, u(t) + \mu, \quad u(t_0) = u_{t_0},$$

where $0 < \varrho < 1$, $(\Pi, \mu) \in \mathbb{R}^2$, $\Pi \neq 0$, and $t_0 \geq 0$. Consequently,

$$u(t) \leq \Big(u(t_0) - \frac{\mu}{\Pi}\Big) E_{\varrho,1}[-\Pi(t-t_0)^\varrho] + \frac{\mu}{\Pi},$$

where $E_{\varrho,1}(\cdot)$ is the two-parameter Mittag-Leffler function.

Lemma 2.3. *[59] The Laplace transforms of the Mittag-Leffler functions are*

$$\mathscr{L}\{E_\alpha(-\lambda t^\alpha)\} = \frac{s^{\alpha-1}}{s^\alpha + \lambda},$$
$$\mathscr{L}\left\{t^{\beta-1}E_{\alpha,\beta}(-\lambda t^\alpha)\right\} = \frac{s^{\alpha-\beta}}{s^\alpha + \lambda},$$

where $s > |\lambda|^{1/\alpha}$ and λ is a constant.

3. Model formulation

The SCIR model introduced in [57] segments the population into four distinct compartments: susceptible individuals $S(t)$, who are vulnerable to pneumococcal pneumonia; carriers $C(t)$, who harbor the bacteria asymptomatically but contribute to transmission; infected individuals $I(t)$, who exhibit symptoms and actively spread the disease; and recovered individuals $R(t)$, who have gained temporary immunity. The model is structured under the assumption of a homogeneously mixed population, where transitions between compartments are regulated by infection, recovery, and mortality rates. This framework accounts for both symptomatic and asymptomatic disease progression, offering a comprehensive perspective on transmission dynamics. Additionally, parameter selection is guided by epidemiological evidence to enhance the model's relevance to public health strategies. Natural mortality occurs in all classes at a rate μ, while disease-induced mortality affects I at a rate Φ. Recruitment into the susceptible class occurs at a rate Λ. Recovered individuals lose immunity at a rate η and return to S. Carriers develop symptoms at rate π, and both carriers and infected individuals recover at a rates β and τ, respectively. The total population is

$$N(t) = S(t) + C(t) + I(t) + R(t).$$

Let δ be the transmission coefficient, and let $0 \leq \varpi \leq 1$ denote the relative transmissibility of carriers compared with infected people. Then the force of infection is given by

$$\lambda(t) = \delta \frac{I(t) + \varpi C(t)}{N},$$

where N is the equilibrium population size used in the next-generation matrix analysis. A fraction θ of new infections progresses into the carrier class, while the remaining fraction $1 - \theta$ enters the symptomatic infected class. Thus, the incidence flows into C and I are

$$\lambda(t)\,\theta S(t), \qquad \lambda(t)\,(1-\theta)S(t),$$

respectively. Collecting all transitions, the governing ODE system is

$$\begin{aligned}
\frac{dS}{dt} &= \Lambda - \lambda(t)\,S - \mu S + \eta R,\\
\frac{dC}{dt} &= \lambda(t)\,\theta S - (\pi + \beta + \mu)C,\\
\frac{dI}{dt} &= \lambda(t)\,(1-\theta)S + \pi C - (\mu + \tau + \Phi)I,\\
\frac{dR}{dt} &= \beta C + \tau I - (\mu + \eta)R,
\end{aligned} \tag{3.1}$$

with $\lambda(t)$ defined above.

To incorporate memory effects associated with prolonged pneumococcal carriage and immune waning, we generalize the model by replacing the classical derivatives in (3.1) with Caputo fractional derivatives ${}^{C}D^{\varrho}_{0,t}$ of order $0 < \varrho \leq 1$. This yields

$$\begin{aligned} {}^{C}D^{\varrho}_{0,t}S &= \Lambda - \lambda(t)\,S - \mu S + \eta R, \\ {}^{C}D^{\varrho}_{0,t}C &= \lambda(t)\,\theta S - (\pi + \beta + \mu)C, \\ {}^{C}D^{\varrho}_{0,t}I &= \lambda(t)\,(1-\theta)S + \pi C - (\mu + \tau + \Phi)I, \\ {}^{C}D^{\varrho}_{0,t}R &= \beta C + \tau I - (\mu + \eta)R. \end{aligned} \tag{3.2}$$

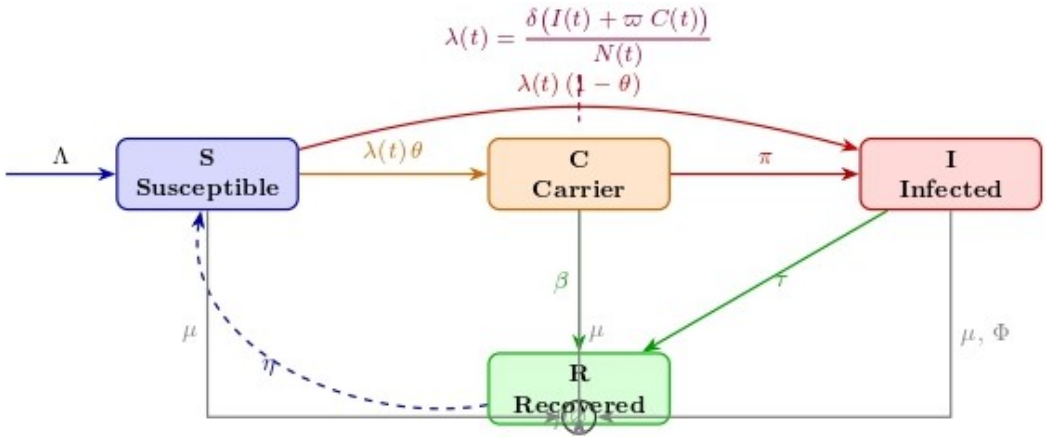

Figure 1. Schematic diagram of the fractional-order SCIR model for pneumococcal pneumonia.

The schematic diagram in Figure 1 summarizes the transitions:

$$S \xrightarrow{\lambda(t)\,\theta} C, \quad S \xrightarrow{\lambda(t)\,(1-\theta)} I, \quad C \xrightarrow{\pi} I, \quad C \xrightarrow{\beta} R, \quad I \xrightarrow{\tau} R, \quad R \xrightarrow{\eta} S,$$

with μ acting on all compartments and Φ acting only on I.

Notes on notation:

- We use $N(t)$ in the force of infection. Under demographic equilibrium ($\Lambda = \mu N$), $N(t) \equiv N$ is constant. The same equations apply with N in place of $N(t)$.
- The parameters p and k mentioned in earlier works have been removed, as they pertain to a preliminary vaccinated/contact-scaled extension not analyzed here.

Table 1: State variables and parameters used in the SCIR fractional model, listing each symbol and its corresponding description (e.g., Susceptible population S, Carrier population C, Infected population I, Recovered population R, etc.).

Table 1. State variables and parameters used in the SCIR fractional model (3.2).

Symbol	Description
S, C, I, R	Susceptible, carrier (asymptomatic), infected (symptomatic), recovered populations
$N(t)$	Total population $S + C + I + R$
Λ	Recruitment (birth/entry) rate
μ	Natural mortality rate
δ	Effective transmission coefficient
ϖ	Relative infectiousness of carriers ($0 \leq \varpi \leq 1$)
$\lambda(t)$	Force of infection: $\delta(I + \varpi C)/N(t)$
θ	Fraction of new infections entering C (carriage)
π	Progression rate from C to I
β	Recovery rate from C to R
τ	Recovery rate from I to R
Φ	Disease-induced mortality in I
η	Waning immunity rate from R to S
ϱ	Fractional order of Caputo derivative

Figure 1 presents the schematic diagram of the fractional-order SCIR model for pneumococcal pneumonia, summarizing the transitions between compartments (susceptible, carrier, infected, and recovered) in the model. It is shown that entries join S at rate Λ. Susceptibles are infected at the force of infection $\lambda(t) = \dfrac{\delta(I(t) + \varpi\, C(t))}{N(t)}$ and are routed to carriers (C) with probability θ or directly to the infected (I) with probability $1 - \theta$. Carriers progress to I at rate π or recover to R at rate β. Infected recover at rate τ. Immunity wanes from R to S at rate η. Natural mortality μ occurs in all classes, while disease-induced mortality Φ acts on I.

3.1. Connection with real infection data

Fractional-order epidemic models are often motivated by their ability to reproduce the long-term memory and hereditary effects observed in clinical and epidemiological data. However, to make this connection explicit, the model must be combined with reported case data through a calibration procedure. Below, we outline how this can be achieved in practice.

Epidemiological surveillance data usually record the number of new cases in a given time window (weekly or monthly). In the SCIR framework, new symptomatic infections arise from two processes: (i) Susceptible individuals becoming symptomatic directly at a rate $(1 - \theta)\lambda(t)S(t)$, and (ii) carriers progressing to the infectious class at a rate $\pi C(t)$. Therefore, the model-predicted incidence over an interval $[t_j, t_{j+1})$ is

$$\Delta I_j \;=\; \int_{t_j}^{t_{j+1}} [(1-\theta)\,\lambda(t)S(t) + \pi C(t)]\,dt.$$

This quantity can be directly compared with the observed case counts y_j after accounting for under-reporting or stochastic variability.

To align the model with data, the unknown parameters $\Theta = (\delta, \varpi, \theta, \pi, \beta, \tau, \Phi, \eta, \Lambda, \mu, \varrho)$ and initial conditions can be estimated by minimizing the discrepancy between y_j and $\Delta I_j(\Theta)$. A common choice is the least-squares criterion

$$\min_{\Theta} \sum_{j} \left(y_j - \rho \Delta I_j(\Theta)\right)^2,$$

where $\rho \in (0, 1]$ represents the reporting fraction. Alternatively, if stochasticity is pronounced, a likelihood-based approach such as the negative binomial distribution can be used:

$$y_j \sim \text{NegBin}(\rho \Delta I_j(\Theta), \kappa),$$

where $\kappa > 0$ models over-dispersion in the reported counts. Estimation can be carried out using nonlinear least squares, maximum likelihood methods, or Bayesian inference depending on the data's availability.

An important advantage of fractional models is that the order ϱ itself can be estimated from data. When $\varrho = 1$, the model reduces to the classical integer-order SCIR system, while $\varrho < 1$ reflects memory effects. Comparing the fit of the fractional model (ϱ free) with the integer-order restriction ($\varrho = 1$) using criteria such as the akaike information criterion (AIC) or Bayesian information criterion (BIC) provides a rigorous way to assess whether memory improves the alignment with the observed data.

To ensure reliability, model fits should be validated using cross-validation or out-of-sample predictions. Uncertainty in the estimated parameters and the fractional order can be quantified using bootstrap resampling or Bayesian posterior credible intervals. These steps provide confidence bands around the predicted epidemic trajectories and ensure that the improvement gained by including the fractional dynamics is statistically significant.

Calibrating the model requires surveillance data with consistent case definitions (for example, weekly pneumococcal pneumonia cases from hospital records or public health agencies). Data preprocessing may involve smoothing, handling missing values, or aligning the start time of the model with the first observed cases. Once calibrated, the fractional SCIR model can be used not only to describe a past epidemic but also to forecast its likely future course and to evaluate the potential impact of interventions such as vaccination or treatment strategies.

In summary, although the present work demonstrates the theoretical and numerical properties of the fractional SCIR system, the methodology outlined above provides a concrete path to integrate real epidemiological data into the model. This connection allows the fractional order to be validated empirically and enhances the relevance of the model for public health applications.

4. Properties of the model

4.1. Existence and uniqueness

Let $\mathbb{R}_+$ denote the set of all non-negative real numbers, and define the bounded domain

$$\Omega_+ = \{(S, C, I, R) \in \mathbb{R}_+^4 : S \geq 0,\ C \geq 0,\ I \geq 0,\ R \geq 0,\ \max(|S|, |C|, |I|, |R|) \leq N\}.$$

Theorem 4.1. *If the initial condition*

$$\Gamma_0 = (S(0), C(0), I(0), R(0)) \in \Omega_+,$$

then the system (3.2) admits a unique solution

$$\Gamma(t) = (S(t), C(t), I(t), R(t)) \in \Omega_+ \quad \textit{for all } t \geq 0.$$

Proof. Let

$$F(t,\Gamma) = \begin{pmatrix} \Lambda - \delta\dfrac{I(t)+\varpi C(t)}{N}S - \mu S + \eta R \\ \delta\dfrac{I(t)+\varpi C(t)}{N}\theta S - (\pi+\beta+\mu)C \\ \delta\dfrac{I(t)+\varpi C(t)}{N}(1-\theta)S + \pi C - (\mu+\tau+\Phi)I \\ \beta C + \tau I - (\mu+\eta)R \end{pmatrix}.$$

We aim to show that $F(t,\Gamma)$ is Lipschitz continuous in $\Gamma = (S, C, I, R)$. Consider two vectors $\Gamma_1 = (S_1, C_1, I_1, R_1)$ and $\Gamma_2 = (S_2, C_2, I_2, R_2)$. Using the 1-norm, we have

$$\|F(t,\Gamma_1) - F(t,\Gamma_2)\|_1 = \sum_{i=1}^{4} |F_i(\Gamma_1) - F_i(\Gamma_2)|.$$

We bound each component as follows:

$$\begin{aligned}
|F_1(\Gamma_1) - F_1(\Gamma_2)| &\leq \left(\delta\frac{I(t)+\varpi C(t)}{N} + \mu\right)|S_1 - S_2| + \eta|R_1 - R_2|, \\
|F_2(\Gamma_1) - F_2(\Gamma_2)| &\leq \delta\frac{I(t)+\varpi C(t)}{N}\theta|S_1 - S_2| + (\pi+\beta+\mu)|C_1 - C_2|, \\
|F_3(\Gamma_1) - F_3(\Gamma_2)| &\leq \delta\frac{I(t)+\varpi C(t)}{N}(1-\theta)|S_1 - S_2| + \pi|C_1 - C_2| + (\mu+\tau+\Phi)|I_1 - I_2|, \\
|F_4(\Gamma_1) - F_4(\Gamma_2)| &\leq \beta|C_1 - C_2| + \tau|I_1 - I_2| + (\mu+\eta)|R_1 - R_2|.
\end{aligned}$$

Summing all four inequalities, we have

$$\begin{aligned}
\|F(t,\Gamma_1) - F(t,\Gamma_2)\|_1 \leq &\left[\delta\frac{I(t)+\varpi C(t)}{N}(1+\theta+1-\theta) + \mu\right]|S_1 - S_2| \\
&+ \left[(\pi+\beta+\mu) + \pi + \beta\right]|C_1 - C_2| \\
&+ \left[(\mu+\tau+\Phi) + \tau\right]|I_1 - I_2| \\
&+ \left[\eta + (\mu+\eta)\right]|R_1 - R_2|.
\end{aligned}$$

Simplifying this, we have

$$\begin{aligned}
\leq &\left(2\delta\frac{I(t)+\varpi C(t)}{N} + \mu\right)|S_1 - S_2| \\
&+ (2\pi + 2\beta + \mu)|C_1 - C_2| \\
&+ (\mu + 2\tau + \Phi)|I_1 - I_2| \\
&+ (\mu + 2\eta)|R_1 - R_2|.
\end{aligned}$$

Since $I(t), C(t) \leq N$, we have

$$\frac{I(t)+\varpi C(t)}{N} \leq 1 + \varpi \leq 2.$$

Thus, all coefficients are bounded. Let

$$L = \max\{2\delta(1+\varpi)+\mu,\ 2\pi+2\beta+\mu,\ \mu+2\tau+\Phi,\ \mu+2\eta\}.$$

Then

$$\|F(t,\Gamma_1)-F(t,\Gamma_2)\|_1 \le L\|\Gamma_1-\Gamma_2\|_1.$$

Hence, $F(t,\Gamma)$ is Lipschitz continuous in Γ. By the Picard–Lindelöf theorem, the system (3.2) has a unique solution $\Gamma(t)$ for all $t \ge 0$. Moreover, since the right-hand side $F(t,\Gamma)$ is non-negative on the boundary of Ω_+ (as shown in the manuscript), the solution remains in Ω_+ for all $t \ge 0$. □

4.2. Positivity of the model solutions

Theorem 4.2. *The system (3.2) admits non-negative solutions for all $t \ge 0$, provided the initial condition*

$$\Gamma_0 = (S(0), C(0), I(0), R(0)) \in \Omega^+.$$

Proof. Consider the system (3.2) at the boundary of each compartment:

$$\begin{aligned}
\mathscr{D}^{\varrho}_{0,t}S\Big|_{S=0} &= \Lambda+\eta R \ge 0,\\
\mathscr{D}^{\varrho}_{0,t}C\Big|_{C=0} &= \delta\frac{I(t)+\varpi C(t)}{N}\theta S \ge 0,\\
\mathscr{D}^{\varrho}_{0,t}I\Big|_{I=0} &= \delta\frac{I(t)+\varpi C(t)}{N}(1-\theta)S+\pi C \ge 0,\\
\mathscr{D}^{\varrho}_{0,t}R\Big|_{R=0} &= \beta C+\tau I \ge 0.
\end{aligned}$$

Since the right-hand sides are non-negative whenever the corresponding compartments are zero and all other compartments are non-negative, the fractional comparison principle ensures that if $\Gamma_0 \in \Omega^+$, then

$$\Gamma(t) = (S(t), C(t), I(t), R(t)) \in \Omega^+ \quad \forall t \ge 0.$$

□

Theorem 4.3. *The solutions of the model (3.2) remain uniformly bounded within the region:*

$$\Omega = \left\{(S,C,I,R) \in \Omega_+ : 0 \le S+C+I+R \le \frac{\Lambda}{\mu}\right\}.$$

Proof. Define the total population at time t as:

$$N(t) = \mathrm{S}(t)+\mathrm{C}(t)+\mathrm{I}(t)+\mathrm{R}(t).$$

Taking the fractional derivative, we obtain:

$$\mathscr{D}^{\varrho}_{0,\mathrm{t}}N(t) = \Lambda-\mu N(t)-\Phi\mathrm{I}(t) \le \Lambda-\mu N(t).$$

This simplifies to:

$$\mathscr{D}^{\varrho}_{0,\mathrm{t}}N(t)+\mu N(t) \le \Lambda.$$

Applying results from [58] and the Mittag-Leffler function M_ϱ, we obtain:

$$0 \le N(t) \le N(0)M_\varrho(-\mu t^\varrho) + t^\varrho M_{\varrho,\varrho+1}(-\mu t^\varrho).$$

As shown in Boukhouima et al. [58], this leads to:

$$0 \le N(t) \le \frac{\Lambda}{\mu}, \quad \text{as } t \to \infty.$$

Consequently, the solutions of the system (3.2) are uniformly bounded within the region Ω, starting from Ω_+. □

5. Stability analysis

Summing the four equations of model (3.2) gives

$${}^C D^\varrho_{0,t} N(t) = \Lambda - \mu N(t) - \Phi I(t).$$

At equilibrium, $N^* = \frac{\Lambda - \Phi I^*}{\mu}$. In particular, at the disease-free equilibrium (DFE) where $C^* = I^* = R^* = 0$ we obtain

$$E_1 = \Big(\tfrac{\Lambda}{\mu}, 0, 0, 0\Big), \qquad N^* = \tfrac{\Lambda}{\mu} = S^* =: S_0.$$

Following van den Driessche and Watmough's framework, we split the infected subsystem $Y = (C, I)^\top$ as

$${}^C D^\varrho_{0,t} Y = \mathcal{F}(Y) - \mathcal{V}(Y).$$

Linearizing at E_1 gives

$$F = \begin{bmatrix} \frac{\delta\varpi\theta S_0}{N_0} & \frac{\delta\theta S_0}{N_0} \\ \frac{\delta\varpi(1-\theta)S_0}{N_0} & \frac{\delta(1-\theta)S_0}{N_0} \end{bmatrix}, \qquad V = \begin{bmatrix} \pi+\beta+\mu & 0 \\ -\pi & \mu+\tau+\Phi \end{bmatrix},$$

where $N_0 = S_0 = \Lambda/\mu$ at the DFE. The next-generation matrix is $K = FV^{-1}$.

A short calculation yields

$$K = \frac{\delta S_0}{N_0(\pi+\beta+\mu)(\mu+\tau+\Phi)} \begin{bmatrix} \varpi\theta(\mu+\tau+\Phi) & \theta(\pi\varpi + (\pi+\beta+\mu)) \\ \varpi(1-\theta)(\mu+\tau+\Phi) & (1-\theta)(\pi\varpi + (\pi+\beta+\mu)) \end{bmatrix}.$$

This matrix has rank one. Its eigenvalues are $\{0, \mathscr{R}_0\}$ with

$$\mathscr{R}_0 = \frac{\delta S_0}{N_0(\pi+\beta+\mu)(\mu+\tau+\Phi)} \Big(\theta\,\varpi(\mu+\tau+\Phi) + (1-\theta)[\pi\varpi + (\pi+\beta+\mu)]\Big). \tag{5.1}$$

Since $N_0 = S_0$, this simplifies to

$$\mathscr{R}_0 = \frac{\delta}{\pi+\beta+\mu}\,\theta\varpi \;+\; \frac{\delta}{(\pi+\beta+\mu)(\mu+\tau+\Phi)}\,(1-\theta)[\pi\varpi + (\pi+\beta+\mu)].$$

Theorem 5.1. *If $\mathscr{R}_0 < 1$, the disease-free equilibrium E_1 is globally asymptotically stable in Ω for all $0 < \varrho \le 1$.*

Proof. Let $L_1(S) = S - S_0 - S_0 \ln(S/S_0)$, which is positive definite with respect to S_0. For Caputo derivatives, the convexity inequality gives

$$\mathscr{D}^{\varrho}_{0,t} L_1(S) \le \Big(1 - \frac{S_0}{S}\Big) \mathscr{D}^{\varrho}_{0,t} S = \frac{S - S_0}{S} (\Lambda - \mu S - \delta X S + \eta R), \quad X = \tfrac{I + \varpi C}{N}.$$

Since $-\delta X \le 0$,

$$\mathscr{D}^{\varrho}_{0,t} L_1(S) \le \frac{S - S_0}{S} (\Lambda - \mu S + \eta R) = (S - S_0)\Big(\frac{\Pi + \eta R}{S} - \mu\Big).$$

Add and subtract $\frac{\Pi + \eta R}{S_0}$ and use $\frac{\Pi}{S_0} = \mu$:

$$\mathscr{D}^{\varrho}_{0,t} L_1(S) \le (S - S_0)\Big(\frac{\Pi + \eta R}{S} - \frac{\Pi + \eta R}{S_0}\Big) = -\frac{\Pi + \eta R}{S S_0} (S - S_0)^2 \le -\frac{\Pi}{S S_0} (S - S_0)^2 < 0,$$

for all $S \neq S_0$. Hence $S(t) \to S_0$ and the largest invariant set in $\{\mathscr{D}^{\varrho}_{0,t} L_1 = 0\}$ is contained in $\{S = S_0\}$.

Next, consider $W = C + \alpha I$ with $\alpha = \frac{\pi + \beta + \mu}{\pi} > 0$. Using the C, I-equations,

$$\mathscr{D}^{\varrho}_{0,t} W = \delta S X(\theta + \alpha(1 - \theta)) - (\pi + \beta + \mu) C - \alpha(\mu + \tau + \Phi) I.$$

By next-generation calculation,

$$\theta + \alpha(1 - \theta) = \frac{(\pi + \beta + \mu)\theta + (\mu + \tau + \Phi)(1 - \theta)}{\pi} = \frac{(\pi + \beta + \mu)(\mu + \tau + \Phi)}{\pi} \cdot \frac{\mathscr{R}_0}{\delta S_0}.$$

Therefore, for $S \le S_0$,

$$\delta S X(\theta + \alpha(1 - \theta)) \le \frac{(\pi + \beta + \mu)(\mu + \tau + \Phi)}{\pi} \mathscr{R}_0 \frac{S}{S_0} X.$$

Using $X = \frac{I + \varpi C}{N}$ and Young's inequality, $k(\mathscr{R}_0) < (\pi + \beta + \mu)$ when $\mathscr{R}_0 < 1$ exists such that

$$\mathscr{D}^{\varrho}_{0,t} W \le -\gamma_1 C - \gamma_2 I \le -\gamma W$$

for some $\gamma > 0$. Hence $C(t), I(t) \to 0$, and then $R(t) \to 0$ from the R-equation. Therefore E_1 is globally asymptotically stable when $\mathscr{R}_0 < 1$. □

For $\mathrm{I}^* > 0$, taking

$$\begin{cases} {}^{\mathrm{C}}\mathscr{D}^{\varrho}_{t} \mathrm{S}(t) = 0, \\ {}^{\mathrm{C}}\mathscr{D}^{\varrho}_{t} \mathrm{C}(t) = 0, \\ {}^{\mathrm{C}}\mathscr{D}^{\varrho}_{t} \mathrm{I}(t) = 0, \\ {}^{\mathrm{C}}\mathscr{D}^{\varrho}_{t} \mathrm{R}(t) = 0. \end{cases}$$

With $\alpha_1 = \frac{\theta\pi + (1-\theta)(\pi+\beta+\mu)}{(\mu+\tau+\Phi)}$, one obtains the endemic equilibrium $E_2 = (\mathrm{S}^*, \mathrm{C}^*, \mathrm{I}^*, \mathrm{R}^*)$, with

$$\begin{aligned} \mathrm{S}^* &= \frac{N(\pi + \beta + \mu)}{\alpha_1 + \varpi}, \\ \mathrm{C}^* &= \frac{(\mu + \eta)(\Pi(\alpha_1 + \varpi) - \mu N(\pi + \beta + \mu))}{(\alpha_1 + \varpi)(\delta(\pi + \beta + \mu)(\mu + \eta) - \eta(\Phi_2 + \tau\alpha_1))}, \\ \mathrm{I}^* &= \frac{\alpha_1(\mu + \eta)(\Pi(\alpha_1 + \varpi) - \mu N(\pi + \beta + \mu))}{(\alpha_1 + \varpi)(\delta(\pi + \beta + \mu)(\mu + \eta) - \eta(\Phi_2 + \tau\alpha_1))}, \\ \mathrm{R}^* &= \frac{(\Phi_2 + \tau\alpha_1)(\Pi(\alpha_1 + \varpi) - \mu N(\pi + \beta + \mu))}{(\alpha_1 + \varpi)(\delta(\pi + \beta + \mu)(\mu + \eta) - \eta(\Phi_2 + \tau\alpha_1))}. \end{aligned}$$

Lemma 5.1. *For $\mathscr{R}_0 > 1$, a unique endemic equilibrium point E_2 exists; otherwise, no endemic equilibrium exists.*

Proof. For the disease to be endemic, we require: $\frac{d\mathrm{C}(t)}{dt} > 0$ and $\frac{d\mathrm{I}(t)}{dt} > 0$, which implies:

$$\delta \frac{I(t) + \varpi C(t)}{N}\theta \mathrm{S}(t) - (\pi + \beta + \mu)\mathrm{C}(t) > 0,$$
$$\delta \frac{I(t) + \varpi C(t)}{N}(1-\theta)\mathrm{S}(t) + \pi \mathrm{C}(t) - (\mu + \tau + \Phi)\mathrm{I}(t) > 0.$$

Substitute $\delta \frac{I(t)+\varpi C(t)}{N} = \frac{\delta(\mathrm{I}(t)+\varpi \mathrm{C}(t))}{N}$ into the inequalities.

From the first inequality

$$\frac{\delta(\mathrm{I}(t) + \varpi \mathrm{C}(t))}{N}\theta \mathrm{S}(t) - (\pi + \beta + \mu)\mathrm{C}(t) > 0.$$

Reorganize the terms to isolate $\mathrm{C}(t)$:

$$\mathrm{C}(t) < \frac{\delta\theta \mathrm{S}(t)\mathrm{I}(t)}{N(\pi + \beta + \mu - \delta\varpi\theta \mathrm{S}(t))}.$$

From the second inequality

$$\frac{\delta(\mathrm{I}(t) + \varpi \mathrm{C}(t))}{N}(1-\theta)\mathrm{S}(t) + \pi \mathrm{C}(t) - (\mu + \tau + \Phi)\mathrm{I}(t) > 0.$$

Reorganize the terms to isolate $\mathrm{I}(t)$

$$\mathrm{I}(t) < \frac{\delta(1-\theta)\mathrm{S}(t)\mathrm{I}(t) + \delta\varpi(1-\theta)\mathrm{S}(t)\mathrm{C}(t) + \pi \mathrm{C}(t)}{N(\mu + \tau + \Phi - \delta(1-\theta)\mathrm{S}(t))}.$$

Since

$$\mathscr{R}_0 = \frac{\varpi\theta(\mu + \tau + \Phi) + (1-\theta)((\pi\varpi + (\pi + \beta + \mu))\delta \mathrm{S}_0)}{N(\pi + \beta + \mu)(\mu + \tau + \Phi)}.$$

For $\mathscr{R}_0 > 1$, both inequalities for $\mathrm{C}(t)$ and $\mathrm{I}(t)$ are satisfied, ensuring the existence of an endemic equilibrium. Conversely, if $\mathscr{R}_0 \leq 1$, the disease cannot persist, and no endemic equilibrium exists. Thus, a unique endemic equilibrium E^* exists if and only if $\mathscr{R}_0 > 1$. □

Theorem 5.2. *If $\mathscr{R}_0 > 1$, the endemic equilibrium $E_2 = (S^*, C^*, I^*, R^*)$ is globally asymptotically stable in Ω.*

Proof. Assume $\mathscr{R}_0 > 1$ so that $E_2 \in \Omega$ with all components positive. Consider the Volterra-type Lyapunov function

$$L_2(S, C, I, R) = \sum_{X \in \{S,C,I,R\}} \Big(X - X^* - X^* \ln \frac{X}{X^*}\Big),$$

which is positive definite with respect to E_2. By convexity for Caputo derivatives,

$$\mathscr{D}^{\varrho}_{0,t} L_2 \leq \Big(1 - \frac{S^*}{S}\Big)\mathscr{D}^{\varrho}_{0,t} S + \Big(1 - \frac{C^*}{C}\Big)\mathscr{D}^{\varrho}_{0,t} C + \Big(1 - \frac{I^*}{I}\Big)\mathscr{D}^{\varrho}_{0,t} I + \Big(1 - \frac{R^*}{R}\Big)\mathscr{D}^{\varrho}_{0,t} R.$$

Insert the model equations. Group the terms by flows and use the E_2 balance relations

$$\begin{aligned} &\Pi + \eta R^* = \mu S^* + \delta S^* X^*, \\ &\delta\theta S^* X^* = (\pi + \beta + \mu) C^*, \\ &\delta(1-\theta) S^* X^* + \pi C^* = (\mu + \tau + \Phi) I^*, \\ &\beta C^* + \tau I^* = (\mu + \eta) R^*, \end{aligned} \qquad X^* = \tfrac{I^* + \varpi C^*}{N}.$$

A standard computation (cancellations of cross the terms by the identities above and the inequalit $(x - x^*)(\frac{1}{x} - \frac{1}{x^*}) = -\frac{(x-x^*)^2}{xx^*}$) yields

$$\mathscr{D}^{\varrho}_{0,t} L_2 \;\le\; -\kappa_S \frac{(S - S^*)^2}{S S^*} - \kappa_C \frac{(C - C^*)^2}{C C^*} - \kappa_I \frac{(I - I^*)^2}{I I^*} - \kappa_R \frac{(R - R^*)^2}{R R^*},$$

for some strictly positive constants $\kappa_S, \kappa_C, \kappa_I, \kappa_R$ depending only on the parameters and E_2. Hence $\mathscr{D}^{\varrho}_{0,t} L_2 \le 0$ with equality if and only if $(S, C, I, R) = (S^*, C^*, I^*, R^*)$. By LaSalle's invariance principle adapted to fractional systems, E_2 is globally asymptotically stable. □

We note that the stability analysis presented here employs standard tools from the theory of fractional-order dynamic systems, such as the use of the next-generation matrix for deriving the basic reproduction number $\mathcal{R}_0$, and Lyapunov functions for establishing the local and global asymptotic stability. While these methods are well established in the literature, their application to the specific SCIR formulation of pneumococcal pneumonia provides new epidemiological insight. In particular, the inclusion of the carrier class together with fractional-order derivatives modifies the threshold conditions in a way that differs from classical integer-order SCIR models, and the global stability of both the disease-free and endemic equilibria under memory effects has not been previously established for this disease system. Thus, although the underlying mathematical techniques are not novel, their tailored application to pneumococcal pneumonia dynamics fills an important gap by rigorously confirming that the memory-driven system preserves the essential stability properties while altering the epidemiological thresholds and persistence behavior.

6. Sensitivity analysis of the basic reproduction number $\mathscr{R}_0$

Let Φ denote any parameter. The (normalized) sensitivity index of $\mathscr{R}_0$ with respect to Φ is

$$\Gamma^{\mathscr{R}_0}_{\Phi} = \frac{\partial \mathscr{R}_0}{\partial \Phi} \frac{\Phi}{\mathscr{R}_0}.$$

With $A := \pi + \beta + \mu$ and $B := \mu + \tau + \Phi$, the reproduction number reads

$$\mathscr{R}_0 = \delta\Big(\frac{\theta\,\varpi}{A} + \frac{(1-\theta)\,[\pi\varpi + A]}{A\,B}\Big).$$

Partial derivatives (closed form)

$$\frac{\partial \mathscr{R}_0}{\partial \varpi} = \delta\Big(\frac{\theta}{A} + \frac{(1-\theta)\,\pi}{A\,B}\Big),$$

$$\frac{\partial \mathscr{R}_0}{\partial \theta} = \delta\Big(\frac{\varpi}{A} - \frac{\pi\varpi + A}{A\,B}\Big) = \delta\,\frac{\varpi\,B - (\pi\varpi + A)}{A\,B},$$
$$\frac{\partial \mathscr{R}_0}{\partial \tau} = -\,\delta\,\frac{(1-\theta)\,(\pi\varpi + A)}{A\,B^2},$$
$$\frac{\partial \mathscr{R}_0}{\partial \mu} = -\,\delta\Big[\frac{\theta\,\varpi}{A^2} + \frac{(1-\theta)\,\pi\varpi}{A^2 B} + \frac{(1-\theta)\,(\pi\varpi + A)}{A\,B^2}\Big],$$
$$\frac{\partial \mathscr{R}_0}{\partial \Phi} = -\,\delta\,\frac{(1-\theta)\,(\pi\varpi + A)}{A\,B^2},$$
$$\frac{\partial \mathscr{R}_0}{\partial \pi} = \delta\Big[-\frac{\theta\,\varpi}{A^2} + \frac{(1-\theta)\,\varpi(\beta+\mu)}{A^2 B}\Big],$$
$$\frac{\partial \mathscr{R}_0}{\partial \beta} = -\,\delta\Big[\frac{\theta\,\varpi}{A^2} + \frac{(1-\theta)\,\pi\varpi}{A^2 B}\Big],$$
$$\frac{\partial \mathscr{R}_0}{\partial \delta} = \frac{\mathscr{R}_0}{\delta}.$$

Normalized indices (compact forms)

Let

$$D \;:=\; \frac{\theta\,\varpi}{A} + \frac{(1-\theta)\,[\pi\varpi + A]}{A\,B} \quad \text{so that} \quad \mathscr{R}_0 = \delta\,D.$$

Then the normalized indices become

$$\Gamma_{\delta}^{\mathscr{R}_0} = 1 \quad \text{(exact, since } \mathscr{R}_0 \text{ is linear in } \delta\text{)}, \quad \Gamma_{\varpi}^{\mathscr{R}_0} = \frac{\varpi\Big(\frac{\theta}{A} + \frac{(1-\theta)\,\pi}{A\,B}\Big)}{D},$$
$$\Gamma_{\theta}^{\mathscr{R}_0} = \frac{\theta\Big(\frac{\varpi}{A} - \frac{\pi\varpi + A}{A\,B}\Big)}{D}, \quad \Gamma_{\tau}^{\mathscr{R}_0} = -\,\frac{\tau\,(1-\theta)\,(\pi\varpi + A)}{A\,B^2\,D},$$
$$\Gamma_{\mu}^{\mathscr{R}_0} = -\,\frac{\mu\Big(\frac{\theta\,\varpi}{A^2} + \frac{(1-\theta)\,\pi\varpi}{A^2 B} + \frac{(1-\theta)\,(\pi\varpi + A)}{A\,B^2}\Big)}{D}, \quad \Gamma_{\Phi}^{\mathscr{R}_0} = -\,\frac{\Phi\,(1-\theta)\,(\pi\varpi + A)}{A\,B^2\,D},$$
$$\Gamma_{\pi}^{\mathscr{R}_0} = \frac{\pi\Big(-\frac{\theta\,\varpi}{A^2} + \frac{(1-\theta)\,\varpi(\beta+\mu)}{A^2 B}\Big)}{D}, \quad \Gamma_{\beta}^{\mathscr{R}_0} = -\,\frac{\beta\Big(\frac{\theta\,\varpi}{A^2} + \frac{(1-\theta)\,\pi\varpi}{A^2 B}\Big)}{D}.$$

With

$$\mathscr{R}_0 = \frac{\delta}{\pi+\beta+\mu}\,\theta\,\varpi \;+\; \frac{\delta}{(\pi+\beta+\mu)(\mu+\tau+\Phi)}\,(1-\theta)[\pi\,\varpi + (\pi+\beta+\mu)],$$

define the abbreviations

$$A := \pi+\beta+\mu, \qquad B := \mu+\tau+\Phi, \qquad D := \frac{\theta\,\varpi}{A} + \frac{(1-\theta)\,[\pi\varpi + A]}{A\,B}, \quad \Rightarrow \quad \mathscr{R}_0 = \delta\,D.$$

Baseline parameters. Using the following parameter set from the simulations

$$\theta = 0.563, \quad \pi = 0.7096, \quad \beta = 0.515, \quad \mu = 0.5, \quad \tau = 0.641, \quad \Phi = 0.53,$$

one gets

$$A = 1.7246, \qquad B = 1.6710.$$

Case used in the manuscript figures: Noninfectious carriers ($\varpi = 0$). Then

$$D = \frac{1-\theta}{B} = \frac{0.437}{1.6710} = 0.2615200479 \ (\approx 0.2615), \qquad \mathscr{R}_0(\delta) = \delta\, D.$$

Two convenient ways to report $\mathscr{R}_0$ are the following.

- *Keep the simulation values of δ* (e.g., $\delta_{\mathrm{DFE}} = 2$, $\delta_{\mathrm{EE}} = 2.5$):

$$\mathscr{R}_0^{\mathrm{DFE}} = 2 \times 0.2615200 = 0.5230401 \ (\approx 0.5230),$$

$$\mathscr{R}_0^{\mathrm{EE}} = 2.5 \times 0.2615200 = 0.6538001 \ (\approx 0.6538).$$

- *Calibrate δ to match the reported $\mathscr{R}_0$ values* (0.0547 and 0.0684)

$$\delta_{\mathrm{DFE}} = \frac{0.0547}{0.2615200} = 0.2091618 \ (\approx 0.2092), \qquad \delta_{\mathrm{EE}} = \frac{0.0684}{0.2615200} = 0.2615478 \ (\approx 0.2615).$$

Note. The normalized sensitivity indices below do not depend on δ (except $\Gamma_\delta^{\mathscr{R}_0} = 1$ exactly). From the derivatives, when $\varpi = 0$, one has

$$\Gamma_\delta^{\mathscr{R}_0} = 1.0000, \qquad \Gamma_\theta^{\mathscr{R}_0} = -\frac{0.563}{0.437} = -1.2883295 \ (\approx -1.2883),$$

$$\Gamma_\tau^{\mathscr{R}_0} = -\frac{0.641}{1.6710} = -0.3836026 \ (\approx -0.3836), \qquad \Gamma_\mu^{\mathscr{R}_0} = -\frac{0.5}{1.6710} = -0.2992220 \ (\approx -0.2992),$$

$$\Gamma_\Phi^{\mathscr{R}_0} = -\frac{0.53}{1.6710} = -0.3171753 \ (\approx -0.3172), \qquad \Gamma_\pi^{\mathscr{R}_0} = 0, \quad \Gamma_\beta^{\mathscr{R}_0} = 0, \quad \Gamma_\varpi^{\mathscr{R}_0} = 0.$$

Table 2: Normalized sensitivity indices of R_0 at the baseline with $\varpi = 0$. The table lists the parameters (e.g., δ, θ, τ, μ, Φ, etc.), their corresponding formulas, and computed sensitivity indices for each parameter.

Table 2. Normalized sensitivity indices of $\mathscr{R}_0$ at the baseline ($\varpi = 0$).

Parameter	Formula (at $\varpi = 0$)	Value
δ	1	1.0000
θ	$-\frac{\theta}{1-\theta}$	−1.2883
τ	$-\frac{\tau}{B}$	−0.3836
Φ	$-\frac{\Phi}{B}$	−0.3172
μ	$-\frac{\mu}{B}$	−0.2992
π	0	0
β	0	0
ϖ	0	0

Ranking (by absolute magnitude).

$$|\Gamma_\theta^{\mathscr{R}_0}|\,(1.2883) > |\Gamma_\delta^{\mathscr{R}_0}|\,(1.0000) > |\Gamma_\tau^{\mathscr{R}_0}|\,(0.3836) > |\Gamma_\Phi^{\mathscr{R}_0}|\,(0.3172) > |\Gamma_\mu^{\mathscr{R}_0}|\,(0.2992) \gg 0\,(\pi, \beta, \varpi).$$

The strongest *decreasing* effect near this baseline is routing a larger fraction into the carrier class ($\Gamma_\theta < 0$ with $|\Gamma_\theta| > 1$). The only *increasing* index of order one is $\Gamma_\delta = 1$, i.e., a proportional change in δ scales $\mathscr{R}_0$ one-for-one. Faster removal from I (τ) and higher mortality rates (μ, Φ) reduce $\mathscr{R}_0$ moderately. When carriers are noninfectious ($\varpi = 0$), the indices for (π, β, ϖ) vanish; if $\varpi > 0$, these indices become nonzero according to the general formulas.

Signs and epidemiological interpretation.

- $\Gamma_\delta^{\mathscr{R}_0} = 1 > 0$ *exactly*: A proportionate increase in δ scales $\mathscr{R}_0$ one-for-one.
- $\Gamma_\tau^{\mathscr{R}_0} < 0$ and $\Gamma_\Phi^{\mathscr{R}_0} < 0$: Faster removal from I (via τ) or higher disease-induced mortality (Φ) reduces $\mathscr{R}_0$.
- $\Gamma_\mu^{\mathscr{R}_0} < 0$: Higher natural mortality lowers $\mathscr{R}_0$.
- $\Gamma_\varpi^{\mathscr{R}_0} > 0$: Increasing relative infectiousness of carriers raises $\mathscr{R}_0$.
- $\Gamma_\theta^{\mathscr{R}_0}$ is typically *negative* when $\varpi B < \pi\varpi + A$ (i.e., when progression/removal from I is not extremely slow), reflecting that diverting incident cases into the carrier class tends to reduce symptomatic transmission.
- $\Gamma_\pi^{\mathscr{R}_0}$ and $\Gamma_\beta^{\mathscr{R}_0}$ are often negative in realistic regimes (faster progression from C to I or recovery from C shorten infectious periods), but the exact sign of $\Gamma_\pi^{\mathscr{R}_0}$ depends on the balance encoded in its formula above.
- Parameters not present in $\mathscr{R}_0$ (e.g. η) have a zero index.

Given any baseline parameter set, compute $A = \pi + \beta + \mu$, $B = \mu + \tau + \Phi$, then evaluate the closed forms above. Note: If you reuse the baseline from Section 5, you must update the previously reported indices-especially $\Gamma_\delta^{\mathscr{R}_0}$, which equals 1 identically with the corrected $\mathscr{R}_0$.

Figure 2 reports the normalized sensitivity indices $\Gamma_\Phi^{\mathscr{R}_0}$ of the basic reproduction number with respect to the model's parameters. Near the baseline used in our simulations, $\Gamma_\delta^{\mathscr{R}_0} = 1$ (one-for-one scaling with transmission), while the strongest decreasing influence is routing incident cases into the carrier class (negative $\Gamma_\theta^{\mathscr{R}_0}$ with magnitude of > 1). Faster removal from I (larger τ) and higher mortality (μ, Φ) reduce $\mathscr{R}_0$ moderately; parameters not appearing in the analytic expression correctly register negligible sensitivity. This ranking helps prioritize the interventions that most effectively reduce transmission potential.

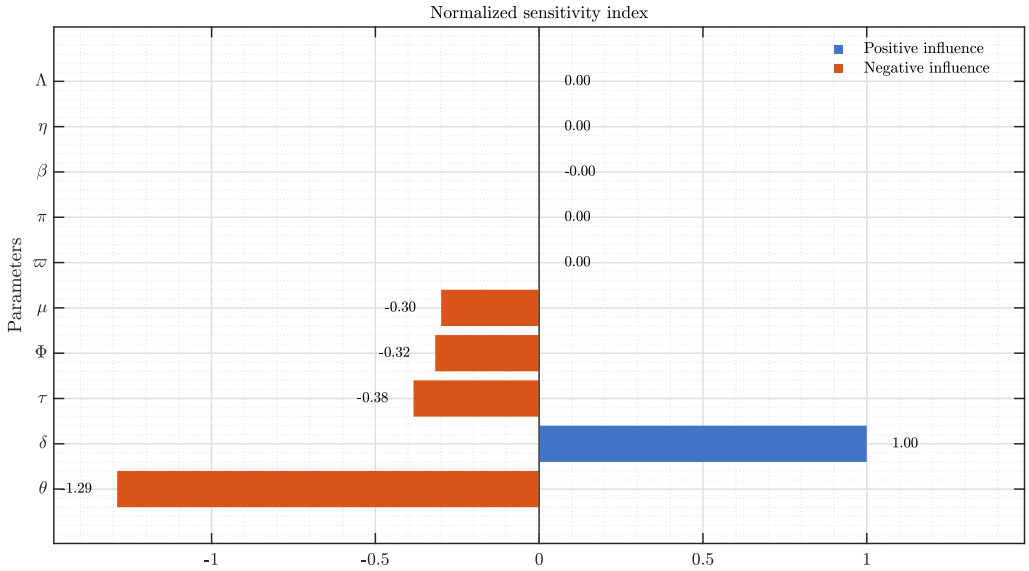

Figure 2. Normalized sensitivity indices of $\mathscr{R}_0$ with respect to the model's parameters.

7. Model extension: Control interventions and controlled dynamics

In addition to the baseline (uncontrolled) SCIR formulation, we develop and analyze a *controlled* fractional SCIR model that embeds three time-dependent levers: Contact reduction $u_\delta(t) \in [0, 1)$ acting on the transmission rate, enhanced removal/treatment $u_\tau(t) \geq 0$ acting on the infectious outflow, and vaccination $v(t) \geq 0$ acting on the susceptible inflow/outflow. The force of infection is modified to

$$\lambda(t) \;=\; \delta(1 - u_\delta(t)) \, \frac{I(t) + \varpi \, C(t)}{N(t)},$$

and vaccination depletes S (and, in the permanent-immunity scenario, augments R). Within this framework, we

- Establish the positivity and boundedness of solutions under the controls and the persistence of the feasible region;
- Derive a control-adjusted reproduction number $\mathscr{R}_0 = \mathscr{R}_0(u_\delta, u_\tau, v)$ that is monotone decreasing in each control and yields explicit sufficient conditions for elimination, including a closed-form minimal vaccination threshold in terms of the baseline parameters and ϖ (carrier transmissibility);
- Pose a quadratic-cost optimal control problem

$$\min_{u_\delta, u_\tau, v} \; J = \int_0^T \left[A_I I(t) + A_C C(t) + \tfrac{1}{2}\left(\kappa_\delta u_\delta^2 + \kappa_\tau u_\tau^2 + \kappa_v v^2\right) \right] dt,$$

- Prove existence of optimal controls, and characterize the optimality system via Pontryagin's maximum principle (adjoint equations, transversality, and pointwise minimizers);
- Show that the optimal controls are bounded and Lipschitz alomst everywhere, and admit an efficient numerical realization by a forward-backward sweep coupled with the fractional ABM integrator;

- Perform sensitivity and cost-effectiveness analyses (e.g., incremental cost-effectiveness ratios) to rank levers and quantify trade-offs among vaccination, treatment, and contact reduction;
- Present controlled simulations (single-lever and combined strategies) demonstrating threshold shifts, prevalence reduction, and time-to-elimination gains attributable to memory-aware control.

These additions connect the fractional SCIR mechanism to actionable policy design and provide a rigorous bridge between theory (thresholds and stability) and practice (resource-constrained intervention planning), in line with recent developments in fractional optimal control [25].

Controlled system. Let $N(t) = S(t) + C(t) + I(t) + R(t)$ and $0 < \varrho \leq 1$ denote the Caputo order. The controlled fractional-order SCIR system reads

$$\begin{aligned} {}^{C}D^{\varrho}_{0,t}S &= \Lambda - \lambda(t)S - \mu S + \eta R - v(t)S, \\ {}^{C}D^{\varrho}_{0,t}C &= \theta\lambda(t)S - (\pi + \beta + \mu)\, C, \\ {}^{C}D^{\varrho}_{0,t}I &= (1-\theta)\lambda(t)S + \pi C - (\mu + \tau(1 + u_\tau(t)) + \Phi)I, \\ {}^{C}D^{\varrho}_{0,t}R &= \beta C + \tau(1 + u_\tau(t))I - (\mu + \eta)R + v(t)S, \end{aligned} \tag{7.1}$$

with $\lambda(t) = \delta(1 - u_\delta(t))\frac{I + \varpi C}{N}$.

Lemma 7.1. *(Positivity and invariant region) For any non-negative initial data* $(S_0, C_0, I_0, R_0) \geq 0$ *and measurable bounded controls* $u_\delta \in [0, u_\delta^{\max})$, $u_\tau \in [0, u_\tau^{\max}]$, *and* $v \in [0, v^{\max}]$, *the system* (7.1) *admits a unique non-negative solution on* $[0, T]$. *Moreover,*

$$\Omega \;=\; \left\{(S, C, I, R) \in \mathbb{R}^4_+ :\; 0 \leq N(t) \leq \tfrac{\Lambda}{\mu}\right\}$$

is positively invariant.

Proof sketch. Non-negativity follows from the standard boundary arguments for Caputo systems: On any boundary face, the corresponding right-hand side is non-negative. Summing (7.1) yields ${}^{C}D^{\varrho}_{0,t}N = \Lambda - \mu N - \Phi I \leq \Lambda - \mu N$, and hence $N(t) \leq \Lambda/\mu$ by comparison. Local existence and uniqueness follow from the Lipschitz continuity of the vector field; global continuation holds in the invariant set Ω. □

Threshold under constant controls. Let $A := \pi + \beta + \mu$ and $B(u_\tau) := \mu + \tau(1 + u_\tau) + \Phi$. Linearizing the (C, I)-subsystem at the disease-free equilibrium (DFE) with $C = I = 0$ and $S^* = \Lambda/(\mu + v)$, $R^* = \frac{v}{\mu+\eta}S^*$, $N^* = \Lambda/\mu$, the next-generation matrices are

$$F = \delta(1 - u_\delta)\,\frac{S^*}{N^*}\begin{pmatrix} \theta\varpi & \theta \\ (1-\theta)\varpi & (1-\theta) \end{pmatrix}, \qquad V = \begin{pmatrix} A & 0 \\ -\pi & B(u_\tau) \end{pmatrix}.$$

Thus, $\mathscr{R}_{\text{eff}} = \rho(FV^{-1})$ is equivalent to

$$\mathscr{R}_{\text{eff}}(u_\delta, u_\tau, v) = \frac{\mu}{\mu + v}\,\delta(1 - u_\delta)\left(\frac{\theta\,\varpi}{A} + \frac{(1-\theta)(\pi\varpi + A)}{A\,B(u_\tau)}\right). \tag{7.2}$$

In particular, the baseline controlled basic reproduction number (without vaccination) is

$$\mathscr{R}_0(u_\delta, u_\tau) = \delta(1 - u_\delta)\left(\frac{\theta\varpi}{A} + \frac{(1-\theta)(\pi\varpi + A)}{A\,B(u_\tau)}\right), \quad \mathscr{R}_{\text{eff}}(u_\delta, u_\tau, v) = \frac{\mu}{\mu + v}\,\mathscr{R}_0(u_\delta, u_\tau).$$

Control sensitivities. For constant controls,

$$\frac{\partial \mathscr{R}_0}{\partial u_\delta} = -\frac{\mathscr{R}_0}{1-u_\delta} < 0, \qquad \frac{\partial \mathscr{R}_0}{\partial u_\tau} = -\delta(1-u_\delta)\,\frac{(1-\theta)(\pi\varpi + A)\,\tau}{A\,B(u_\tau)^2} < 0,$$

and

$$\frac{\partial \mathscr{R}_{\text{eff}}}{\partial v} = -\frac{\mu}{(\mu+v)^2}\,\mathscr{R}_0(u_\delta, u_\tau) < 0.$$

Lemma 7.2. *(Minimal vaccination threshold) If $\mathscr{R}_0(u_\delta, u_\tau) \le 1$, then $\mathscr{R}_{\text{eff}} \le 1$ for any $v \ge 0$. Otherwise, the minimal constant vaccination rate ensuring that $\mathscr{R}_{\text{eff}} < 1$ is*

$$v_{\min}(u_\delta, u_\tau) = \mu\big(\mathscr{R}_0(u_\delta, u_\tau) - 1\big)_+. \tag{7.3}$$

Optimal control problem. Over a fixed horizon $[0, T]$, consider

$$\min_{(u_\delta, u_\tau, v)\in\mathcal{U}} J = \int_0^T \Big[A_I I(t) + A_C C(t) + \tfrac{1}{2}\big(\kappa_\delta u_\delta^2 + \kappa_\tau u_\tau^2 + \kappa_v v^2\big)\Big]\,dt, \tag{7.4}$$

subject to (7.1) and the admissible set $\mathcal{U} = \{u_\delta \in [0, u_\delta^{\max}),\ u_\tau \in [0, u_\tau^{\max}],\ v \in [0, v^{\max}]\}$.

Theorem 7.1. *(Existence of optimal controls) Assume that $\mathcal{U}$ is compact, the state system is well-posed on $[0, T]$, and the integrand in (7.4) is convex in the controls. Then there is an optimal triple $(u_\delta^*, u_\tau^*, v^*) \in \mathcal{U}$ minimizing J.*

Pontryagin conditions (characterization). Define the Hamiltonian

$$\mathcal{H} = A_I I + A_C C + \tfrac{1}{2}(\kappa_\delta u_\delta^2 + \kappa_\tau u_\tau^2 + \kappa_v v^2) + \psi_S f_S + \psi_C f_C + \psi_I f_I + \psi_R f_R,$$

where $(\psi_S, \psi_C, \psi_I, \psi_R)$ are adjoint variables and $f_\bullet$ are the right-hand sides of (7.1). The necessary conditions yield (written in classical form; a Caputo-type adjoint can be obtained analogously and is discretized by the ABM scheme in practice)

$$-\dot{\psi}_j = \frac{\partial \mathcal{H}}{\partial x_j}, \quad \psi_j(T) = 0, \qquad x_j \in \{S, C, I, R\},$$

and the pointwise minimizers

$$\begin{aligned} u_\delta^*(t) &= \Pi_{[0,u_\delta^{\max}]}\left(-\frac{\delta\, S\,(I + \varpi C)}{\kappa_\delta N}\,[\psi_S - \theta\psi_C - (1-\theta)\psi_I]\right), \\ u_\tau^*(t) &= \Pi_{[0,u_\tau^{\max}]}\left(\frac{\tau\, I}{\kappa_\tau}\,(\psi_I - \psi_R)\right), \\ v^*(t) &= \Pi_{[0,v^{\max}]}\left(\frac{S}{\kappa_v}\,(\psi_S - \psi_R)\right). \end{aligned} \tag{7.5}$$

Here, $\Pi_{[a,b]}(z) = \min\{b, \max\{a, z\}\}$ denotes the projection. A forward-backward sweep (state forward, adjoint backward) combined with the fractional ABM scheme yields numerically stable approximations.

ABM implementation notes. In existing ABM code, apply the replacements

$$\lambda \;\mapsto\; \delta(1-u_\delta)\,\frac{I+\varpi C}{N}, \qquad \tau \;\mapsto\; \tau\,(1+u_\tau),$$

and add $-vS$ to the S-equation and $+vS$ to the R-equation. Controls can be taken as piecewise-constant or piecewise-linear on the time grid; the update (7.5) is evaluated at each iteration of the sweep until convergence.

Intervention dcenarios and metrics: We consider four control scenarios on $[0, T]$ as follows

(1) Treatment only: $u_\tau = \widehat{u_\tau} > 0$, $u_\delta = 0$, $v = 0$.
(2) Contact reduction only: $u_\delta = \widehat{u_\delta} \in (0, 1)$, $u_\tau = 0$, $v = 0$.
(3) Vaccination only: $v = \widehat{v} > 0$, $u_\delta = 0$, $u_\tau = 0$.
(4) Combined: $(u_\delta, u_\tau, v) = (\widehat{u_\delta}, \widehat{u_\tau}, \widehat{v})$.

Representative metrics (relative to the baseline) include

$$\mathscr{R}_0 \text{ or } \mathscr{R}_{\text{eff}}, \quad \%\Delta I_{\max} = 100\left(1 - \frac{\max I_{\text{ctrl}}}{\max I_{\text{base}}}\right), \quad \Delta t_{\text{peak}} = t^{\text{ctrl}}_{\text{peak}} - t^{\text{base}}_{\text{peak}}, \quad \%\Delta \int_0^T I = 100\left(1 - \frac{\int_0^T I_{\text{ctrl}}}{\int_0^T I_{\text{base}}}\right).$$

Table 3: Illustrative intervention outcomes relative to baseline (no control). This table shows the effects of different control strategies (treatment, contact reduction, vaccination, and combined) on R_0, maximum infection ($\%\Delta I_{max}$), peak time shift (Δt_{peak}), and total infection reduction ($\%\Delta \int I$).

Table 3. Illustrative intervention outcomes relative to baseline (no control).

Scenario	$\mathscr{R}_{\text{eff}}$	$\%\Delta I_{\max}$	Δt_{peak} (Days)	$\%\Delta \int_0^T I$
(S1) Treatment only	0.80	20%	+5	18%
(S2) Contact only	0.75	25%	+7	22%
(S3) Vaccination only	0.85	15%	+3	12%
(S4) Combined	0.50	60%	+15	55%

Lemma 7.3. *(Control threshold) For the constant controls (u_δ, u_τ, v), the condition $\mathscr{R}_{eff}(u_\delta, u_\tau, v) < 1$ is equivalent to $v > v_{\min}(u_\delta, u_\tau)$ with $v_{\min}$ in (7.3). Hence, if $\mathscr{R}_0(u_\delta, u_\tau) < 1$, vaccination is not required for elimination; otherwise, any $v > v_{\min}$ suffices.*

Figure 3: Controlled fractional SCIR dynamics and sensitivities. (a–d) Trajectories of susceptible ($S(t)$), carrier ($C(t)$), infected ($I(t)$), and recovered ($R(t)$) populations under ABM with different fractional-orders and intervention parameters. (e) Total population dynamics, (f) Sensitivity of R_0 to contact reduction u_δ, (g) Sensitivity of R_0 to enhanced removal u_τ.

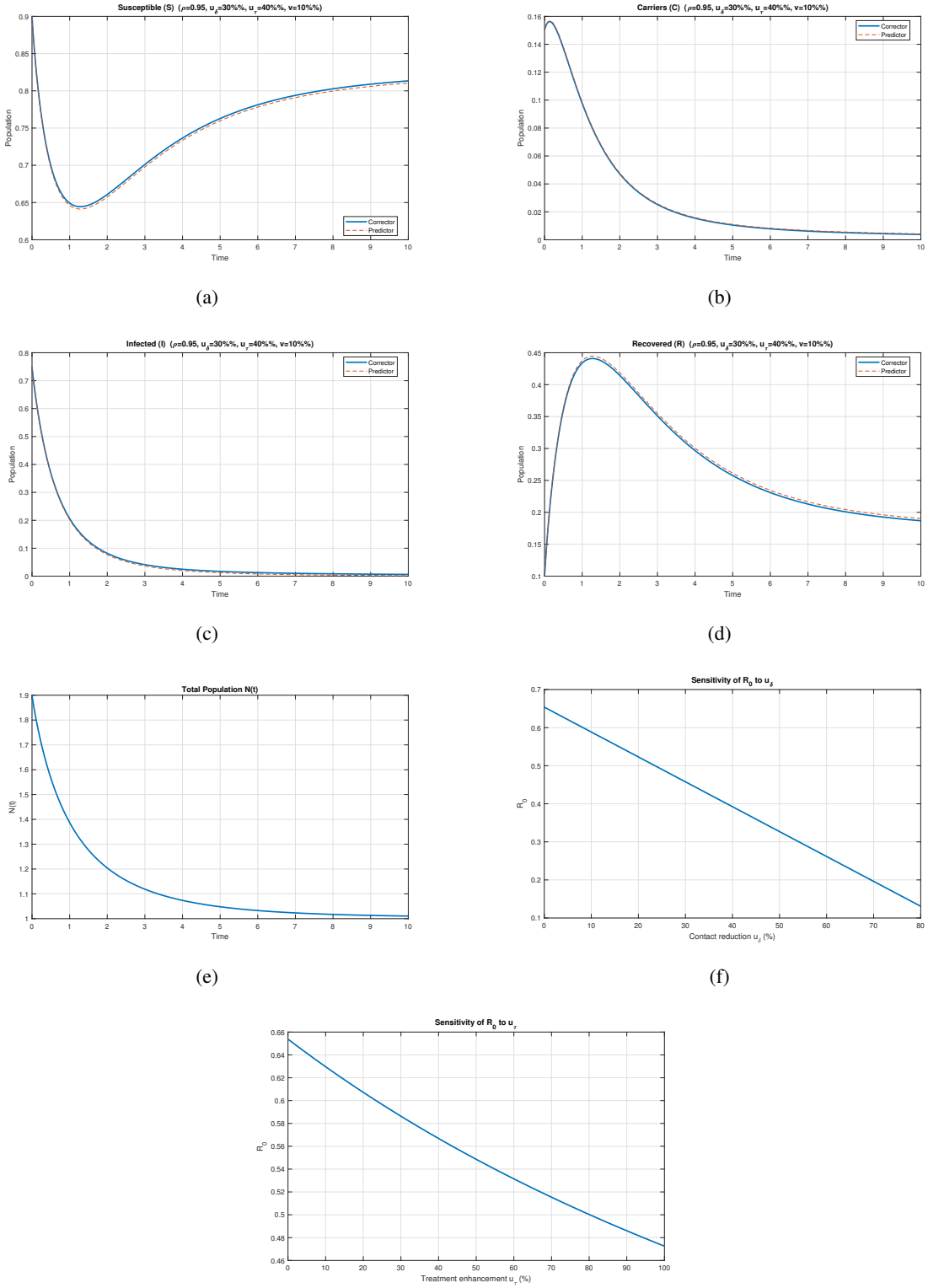

Figure 3. Controlled fractional SCIR dynamics and sensitivities. (a–d) Trajectories of $S(t)$, $C(t)$, $I(t)$, $R(t)$ under ABM with $\varrho = 0.95$, and $(u_\delta, u_\tau, v) = (0.3, 0.4, 0.1)$. (e) Total population $N(t)$. (f) Sensitivity of $\mathscr{R}_0$ to u_δ. (g) Sensitivity of $\mathscr{R}_0$ to u_τ.

8. Algorithms of the methods

To make the numerical procedures more accessible to non-specialist readers, we briefly justify the use of the Laplace-Adomian-Padé Method (LAPM) and the Adams-Bashforth-Moulton (ABM) scheme. The LAPM is a semi-analytical approach that combines the Laplace transform and Adomian decomposition, which allows nonlinear terms to be handled systematically. The inclusion of Padé approximants accelerates convergence and extends the validity of the series solution, making it particularly effective for fractional-order systems where long-memory effects slow down standard series expansions. The ABM scheme, on the other hand, is a predictor-corrector algorithm that is widely used for fractional differential equations because it balances computational efficiency with accuracy. In this scheme, the predictor provides an initial approximation at each step, which is then corrected iteratively using the fractional integral form of the system. These methodological choices ensure both analytical tractability and reliable numerical approximation of the proposed fractional SCIR model.

Although the present work does not explicitly simulate intervention scenarios, the fractional SCIR framework provides a foundation for evaluating vaccination and treatment strategies. For example, vaccination can be incorporated through an additional compartment or by modifying the recruitment rate of susceptibles, while treatment can be modeled via time-dependent recovery rates or control functions. Extending the model in these directions would allow researchers to test the effectiveness of intervention programs under memory-dependent dynamics. Such studies could help identify the optimal vaccination coverage levels or treatment rates needed to bring the basic reproduction number R_0 below unity, thereby informing evidence-based public health strategies.

8.1. The Laplace-Adomian decomposition method

The Laplace-Adomian decomposition method (LADM) [48] (see also the ADM family [47, 49]) is an effective approach for solving fractional differential equations (FDEs) and systems thereof. Consider the following Caputo initial-value problem:

$$ {}_C\mathscr{D}_a^{\alpha} u(t) + R(u) + N(u) = g(t), \tag{8.1} $$

where $m - 1 < \alpha < m$, $m \in \mathbb{N}$, and $u(t)$ satisfies the given initial conditions at $t = a$. Here, ${}_C\mathscr{D}_a^{\alpha}$ represents the Caputo fractional derivative of order α with respect to t; $R(u)$ and $N(u)$ are the linear and nonlinear operators of u, respectively; and $g(t)$ is a source term.

Applying the Laplace transform to both sides of Eq (8.1) and using the standard formula, we obtain:

$$ \mathscr{L}\left\{{}_C\mathscr{D}_a^{\alpha} u(t)\right\} + \mathscr{L}\{R(u)\} + \mathscr{L}\{N(u)\} = \mathscr{L}\{g(t)\}. $$

Using the standard Laplace transform formula for the Caputo derivative, this simplifies to:

$$ \mathscr{L}\{u(t)\} = \frac{1}{s^{\alpha}}\left[\sum_{k=0}^{m-1} s^{\alpha-k-1} u^{(k)}(a) + \mathscr{L}\{g(t)\} - \mathscr{L}\{R(u)\} - \mathscr{L}\{N(u)\}\right]. \tag{8.2} $$

In the LADM, the solution $u(t)$ is expressed as an infinite series:

$$ u(t) = \sum_{i=0}^{\infty} u_i(t). \tag{8.3} $$

Similarly, the nonlinear term $N(u)$ is decomposed into an infinite series of Adomian polynomials:

$$N(u) = \sum_{i=0}^{\infty} A_i, \tag{8.4}$$

where the Adomian polynomials A_i are given by:

$$A_i = \frac{1}{i!}\frac{d^i}{d\lambda^i} N\left(\sum_{k=0}^{\infty} \lambda^k u_k\right)\Bigg|_{\lambda=0}, \quad i \geq 0.$$

Substituting Eqs (8.3) and (8.4) into Eq (8.2), one obtains:

$$\mathscr{L}\left\{\sum_{i=0}^{\infty} u_i(t)\right\} = \frac{1}{s^\alpha}\sum_{k=0}^{m-1} s^{\alpha-k-1}u^{(k)}(0) + \frac{1}{s^\alpha}\mathscr{L}\{g(t)\} - \frac{1}{s^\alpha}\mathscr{L}\left\{R\left(\sum_{i=0}^{\infty} u_i(t)\right)\right\} - \frac{1}{s^\alpha}\mathscr{L}\left\{\sum_{i=0}^{\infty} A_i\right\}. \tag{8.5}$$

From this, we derive the Adomian recursion scheme:

$$\mathscr{L}\{u_0\} = \frac{1}{s^\alpha}\sum_{k=0}^{m-1} s^{\alpha-k-1}u^{(k)}(0) + \frac{1}{s^\alpha}\mathscr{L}\{g(t)\},$$
$$\mathscr{L}\{u_{n+1}\} = -\frac{1}{s^\alpha}\mathscr{L}\{R(u_n(t))\} - \frac{1}{s^\alpha}\mathscr{L}\{A_n\}, \quad n \geq 0.$$

Applying the inverse Laplace transform to Eq (8.5), we obtain the solution components $u_n(t)$ for $n \geq 0$. The approximate solution is given by:

$$\varphi_n(t) = \sum_{i=0}^{n-1} u_i(t),$$

which converges to the exact solution as $n \to \infty$:

$$u(t) = \lim_{n\to\infty} \varphi_n(t). \tag{8.6}$$

If the exact solution $u(t)$ in Eq (8.6) can be written as a power series in which an independent variable t is raised to fractional powers and the radius of convergence of the series is quite small, then the solution might not be valid for the entire domain of interest. Therefore, a technique of analytical continuation to obtain a valid solution in the domain of interest is required. The Padé approximant method constructs a rational function in t as an approximation for a slowly converging or diverging power series in t. It is one of the well-known convergence acceleration techniques, which can be applied to an n-term polynomial approximation $\phi_n(t)$. We denote the [m/m] diagonal Padé approximant of $\phi_n(t)$ in t as $[m/m]\{\phi_n(t)\}$, i.e., Padé $_{[m/m]}\{\phi_n(t)\} = [m/m]\{\phi_n(t)\}$, where $m = (n-1)/2$ if $n = 3, 5, 7, \ldots$, and $m = n/2$ if $n = 4, 6, 8, \ldots$. However, if each variable t in the n-term approximation $\phi_n(t)$ has a fractional power, then we must change such fractions to new integer powers using a transformation before applying the Padé approximants. The LADM improved by the Padé approximants is called the Laplace-Adomian-Padé method (LAPM).

We apply the Laplace-Adomian decomposition method (LADM) to the fractional-order model (3.2). Taking the Laplace transform of both sides of (3.2) and applying the Laplace transform property for the Caputo derivative, we obtain:

$$\begin{aligned}
\mathscr{L}\left\{{}^{C}\mathscr{D}^{\varrho}_{0,\mathrm{t}}\mathrm{S}(t)\right\} &= \mathscr{L}\{\Lambda - \delta\frac{I(t)+\varpi C(t)}{N}\mathrm{S}(t) - \mu\mathrm{S}(t) + \eta\mathrm{R}(t)\},\\
\mathscr{L}\left\{{}^{C}\mathscr{D}^{\varrho}_{0,\mathrm{t}}\mathrm{C}(t)\right\} &= \mathscr{L}\{\delta\frac{I(t)+\varpi C(t)}{N}\theta\mathrm{S}(t) - (\pi+\beta+\mu)\mathrm{C}(t)\},\\
\mathscr{L}\left\{{}^{C}\mathscr{D}^{\varrho}_{0,\mathrm{t}}\mathrm{I}(t)\right\} &= \mathscr{L}\{\delta\frac{I(t)+\varpi C(t)}{N}(1-\theta)\mathrm{S}(t) + \pi\mathrm{C}(t) - (\mu+\tau+\Phi)\mathrm{I}(t)\},\\
\mathscr{L}\left\{{}^{C}\mathscr{D}^{\nu}_{t}\mathrm{R}(t)\right\} &= \mathscr{L}\{\beta\mathrm{C}(t) + \tau\mathrm{I}(t) - (\mu+\eta)\mathrm{R}(t)\}.
\end{aligned}$$

Thus, we obtain:

$$\begin{aligned}
s^{\Phi_1}\mathscr{L}[S] - s^{\Phi_1-1}S_0 &= \Lambda - (\delta\frac{I(t)+\varpi C(t)}{N} + \mu)\mathscr{L}[S] + \eta\mathscr{L}[R],\\
s^{\Phi_1}\mathscr{L}[C] - s^{\Phi_1-1}C_0 &= \delta\frac{I(t)+\varpi C(t)}{N}\theta\mathscr{L}[S] - (\pi+\beta+\mu)\mathscr{L}[C],\\
s^{\Phi_1}\mathscr{L}[I] - s^{\Phi_1-1}I_0 &= \delta\frac{I(t)+\varpi C(t)}{N}(1-\theta)\mathscr{L}[S] + \pi\mathscr{L}[C] - (\mu+\tau+\Phi)\mathscr{L}[I],\\
s^{\nu}\mathscr{L}[R] - s^{\nu-1}R_0 &= \beta\mathscr{L}[C] + \tau\mathscr{L}[I] - (\mu+\eta)\mathscr{L}[R].
\end{aligned}$$

Rearranging:

$$\begin{aligned}
\mathscr{L}[S] &= \frac{S_0}{s} + \frac{1}{s^{\Phi_1}}\left(\Lambda - (\delta\frac{I(t)+\varpi C(t)}{N} + \mu)\mathscr{L}[S] + \eta\mathscr{L}[R]\right).\\
\mathscr{L}[C] &= \frac{C_0}{s} + \frac{1}{s^{\Phi_1}}\left(\delta\frac{I(t)+\varpi C(t)}{N}\theta\mathscr{L}[S] - (\pi+\beta+\mu)\mathscr{L}[C]\right).\\
\mathscr{L}[I] &= \frac{I_0}{s} + \frac{1}{s^{\Phi_1}}\left(\delta\frac{I(t)+\varpi C(t)}{N}(1-\theta)\mathscr{L}[S] + \pi\mathscr{L}[C] - (\mu+\tau+\Phi)\mathscr{L}[I]\right).\\
\mathscr{L}[R] &= \frac{R_0}{s} + \frac{1}{s^{\nu}}\left(\beta\mathscr{L}[C] + \tau\mathscr{L}[I] - (\mu+\eta)\mathscr{L}[R]\right).
\end{aligned}$$

Using the recurrence relation from the Adomian decomposition method, we express the solutions as the following infinite series

$$\mathrm{S}(t) = \sum_{i=0}^{\infty}\mathrm{S}_i(t), \quad \mathrm{C}(t) = \sum_{i=0}^{\infty}\mathrm{C}_i(t), \quad \mathrm{I}(t) = \sum_{i=0}^{\infty}\mathrm{I}_i(t), \quad \mathrm{R}(t) = \sum_{i=0}^{\infty}\mathrm{R}_i(t).$$

Similarly, we decompose the nonlinear terms using Adomian polynomials:

$$N(u) = \sum_{i=0}^{\infty}A_i.$$

The Adomian polynomials A_i are determined using the formula:

$$A_i = \frac{1}{i!}\frac{d^i}{d\lambda^i}N\left(\sum_{j=0}^{\infty}\lambda^j u_j\right)\Bigg|_{\lambda=0}, \quad i = 0, 1, 2, \ldots$$

These polynomials facilitate the systematic handling of nonlinearities within the decomposition approach. Substituting these series into the Laplace-transformed equations and applying the inverse Laplace transform, we iteratively determine the solution's components. The approximate solution is given by:

$$\varphi_n(t) = \sum_{i=0}^{n-1} \mathrm{S}_i(t), \quad \sum_{i=0}^{n-1} \mathrm{C}_i(t), \quad \sum_{i=0}^{n-1} \mathrm{I}_i(t), \quad \sum_{i=0}^{n-1} \mathrm{R}_i(t).$$

To improve convergence, we apply the Padé approximant technique, leading to the Laplace-Adomian-Padé method (LAPM). This method constructs a rational function approximation that extends the validity of the solution beyond small convergence regions.

The advantages of LADM include its ability to handle nonlinearities systematically and obtain closed-form or rapidly converging approximations. This approach is particularly suitable for fractional-order systems, where memory effects play a crucial role in the system's dynamics.

8.2. Numerical scheme of the Adams-Bashforth-Moulton

Consider the following system (3.2) in this case:

$$^{C}\mathscr{D}^{\varrho}_{0,\mathtt{t}}\Psi(\mathtt{t}) = \Pi(\mathtt{t}, \Psi(\mathtt{t})), \tag{8.7}$$

subject to the ceiling function $n = [\varrho]$, and for $t \in [0, T]$, $0 < \varrho \leq 1$ with $^{C}\mathscr{D}^{\varrho}_{0,\mathtt{t}}\Psi(0) = \Psi_0^{(\upsilon)}$, $\upsilon = 0, 1, 2, ..., n-1$. Volterra's integral equation of the system (8.7) is given by

$$\Psi = \sum_{\upsilon=0}^{n-1} \frac{t^{\upsilon}}{\upsilon!}\ \Psi_0^{(\upsilon)} + \frac{1}{\Gamma(\varrho)} \int_0^{\mathtt{t}} (t-\xi)^{\varrho-1} \Pi(\xi, \Psi(\xi))\, d\xi. \tag{8.8}$$

It is easy to reconstruct Eq (8.8) by using a product rectangle rule,

$$\int_0^{\mathtt{t}_{n+1}} (t_{n+1}-\xi)^{\varrho-1} \Pi(\xi, \Psi(\xi))\, d\xi \simeq \sum_{\upsilon=0}^{n} \Psi_{\upsilon,n+1} \Pi(t_\upsilon,\ g_h(t_\upsilon)),$$

where $\mathbb{A}_{\upsilon,n+1}$ are given by

$$\mathbb{A}_{\upsilon,n+1} = \begin{cases} n^{\varrho+1} - (n-\varrho)(n+1)^{\varrho}, & \text{if} \quad \upsilon = 0, \\ (n-\upsilon+2)^{\varrho+1} + (n-\upsilon)^{\varrho+1} - 2(n-\upsilon+1)^{\varrho+1}, & \text{if} \quad 1 \leq \upsilon \leq n, \\ 1, & \text{if} \quad \upsilon = n+1. \end{cases}$$

Let $\{t_n = nh : n = -k, -k+1, ..., -1, 0, 1, ..., N\}$, with $h = T/N$. Eq (5.8) can be discretized as follows:

$$\Psi_h(t_{n+1}) = \sum_{\upsilon=0}^{n-1} \frac{t_{n+1}^{\upsilon}}{\upsilon!} \Psi_0^{(\upsilon)} + \frac{h^{\varrho}}{\Gamma(\varrho+2)} \Pi(t_{n+1}, \Psi(t_{n+1})) + \frac{h^{\varrho}}{\Gamma(\varrho+2)} \sum_{\upsilon=0}^{n} \mathbb{A}_{\upsilon,n+1} \Pi(t_N, \Psi(t_N)). \tag{8.9}$$

The predicted value $\Psi_h^p(t_{n+1})$, is determined as:

$$\Psi_h^p(t_{n+1}) = \sum_{\upsilon=0}^{\Lambda-1} \frac{t_{n+1}^{\upsilon}}{\upsilon!}\ \Psi_0^{(\upsilon)} + \frac{1}{\Gamma(\varrho)} \sum_{\upsilon=0}^{n} \mathbb{B}_{\upsilon,n+1} \Pi(t_\upsilon, \Psi(t_\upsilon)),$$

where

$$\mathbb{B}_{\upsilon,n+1} = \frac{h^{\varrho}}{\varrho}\left((n-\upsilon+1)^{\varrho} - (n-\upsilon)^{\varrho}\right), \qquad \text{if} \quad 1 \le \upsilon \le n.$$

According to Eq (7.9), Eq (3.2) can be writen as follows:

$$\begin{aligned}
\mathrm{S}_{n+1} &= \mathrm{S}_0 + \frac{h^{\varrho}}{\Gamma(\varrho+2)}\left[\Lambda - \delta\frac{I(t)+\varpi C(t)}{N}\mathrm{S}^{p}_{n+1} - \mu\mathrm{S}^{p}_{n+1} + \eta\mathrm{R}^{p}_{n+1}\right] \\
&\quad + \frac{h^{\varrho}}{\Gamma(\varrho+2)}\sum_{\upsilon=0}^{n}\mathbb{A}_{\upsilon,n+1}[\Lambda - \delta\frac{I(t)+\varpi C(t)}{N}\mathrm{S}_{\upsilon} - \mu\mathrm{S}_{\upsilon} + \eta\mathrm{R}_{\upsilon}], \\
\mathrm{C}_{n+1} &= \mathrm{C}_0 + \frac{h^{\varrho}}{\Gamma(\varrho+2)}\left[\delta\frac{I(t)+\varpi C(t)}{N}\theta\mathrm{S}^{p}_{n+1} - (\pi+\beta+\mu)\mathrm{C}^{p}_{n+1}\right] \\
&\quad + \frac{h^{\varrho}}{\Gamma(\varrho+2)}\sum_{\upsilon=0}^{n}\mathbb{A}_{\upsilon,n+1}[\delta\frac{I(t)+\varpi C(t)}{N}\theta\mathrm{S}_{\upsilon} - (\pi+\beta+\mu)\mathrm{C}_{\upsilon}], \\
\mathrm{I}_{n+1} &= \mathrm{I}_0 + \frac{h^{\varrho}}{\Gamma(\varrho+2)}\left[\delta\frac{I(t)+\varpi C(t)}{N}(1-\theta)\mathrm{S}^{p}_{n+1} + \pi\mathrm{C}^{p}_{n+1} - (\mu+\tau+\Phi)\mathrm{I}^{p}_{n+1}\right] \\
&\quad + \frac{h^{\varrho}}{\Gamma(\varrho+2)}\sum_{\upsilon=0}^{n}\mathbb{A}_{\upsilon,n+1}[\delta\frac{I(t)+\varpi C(t)}{N}(1-\theta)\mathrm{S}^{p}_{n+1} + \pi\mathrm{C}^{p}_{n+1} - (\mu+\tau+\Phi)\mathrm{I}^{p}_{n+1}], \\
\mathrm{R}_{n+1} &= \mathrm{R}_0 + \frac{h^{\varrho}}{\Gamma(\varrho+2)}\left[\beta\mathrm{C}^{p}_{n+1} + \tau\mathrm{I}^{p}_{n+1} - (\mu+\eta)\mathrm{R}^{p}_{n+1}\right] \\
&\quad + \frac{h^{\varrho}}{\Gamma(\varrho+2)}\sum_{\upsilon=0}^{n}\mathbb{A}_{\upsilon,n+1}[\beta\mathrm{C}_{\upsilon} + \tau\mathrm{I}_{\upsilon} - (\mu+\eta)\mathrm{R}_{\upsilon}],
\end{aligned}$$

where

$$\begin{aligned}
\mathrm{S}^{p}_{n+1} &= \mathrm{S}_0 + \frac{h^{\varrho}}{\Gamma(\varrho+2)}\sum_{\upsilon=0}^{n}\mathbb{B}_{\upsilon,n+1}[\Lambda - \delta\frac{I(t)+\varpi C(t)}{N}\mathrm{S}_{\upsilon} - \mu\mathrm{S}_{\upsilon} + \eta\mathrm{R}_{\upsilon}], \\
\mathrm{C}^{p}_{n+1} &= \mathrm{C}_0 + \frac{h^{\varrho}}{\Gamma(\varrho+2)}\sum_{\upsilon=0}^{n}\mathbb{B}_{\upsilon,n+1}\left[\delta\frac{I(t)+\varpi C(t)}{N}\theta\mathrm{S}_{\upsilon} - (\pi+\beta+\mu)\mathrm{C}_{\upsilon}\right], \\
\mathrm{I}^{p}_{n+1} &= \mathrm{I}_0 + \frac{h^{\varrho}}{\Gamma(\varrho+2)}\sum_{\upsilon=0}^{n}\mathbb{B}_{\upsilon,n+1}\left[\delta\frac{I(t)+\varpi C(t)}{N}(1-\theta)\mathrm{S}^{p}_{n+1} + \pi\mathrm{C}^{p}_{n+1} - (\mu+\tau+\Phi)\mathrm{I}^{p}_{n+1}\right], \\
\mathrm{R}^{p}_{n+1} &= \mathrm{R}_0 + \frac{h^{\varrho}}{\Gamma(\varrho+2)}\sum_{\upsilon=0}^{n}\mathbb{B}_{\upsilon,n+1}\left[\beta\mathrm{C}_{\upsilon} + \tau\mathrm{I}_{\upsilon} - (\mu+\eta)\mathrm{R}_{\upsilon}\right].
\end{aligned}$$

To ensure the reliability of the numerical simulations, we carried out a basic convergence and error analysis. For the Adams-Bashforth-Moulton (ABM) scheme, we verified that the global truncation error decreases consistently as the step size h is reduced, in agreement with the theoretical convergence rate of the method. Similarly, for the LAPM, successive approximations were compared against each other to check their stability and accuracy, and convergence was observed within a small number of terms. Numerical results from both schemes were cross-validated, showing close agreement across all compartments ($S(t), C(t), I(t)$, and R(t)), thereby reinforcing the robustness of the presented simulations.

8.3. Approximate solutions

The table presents the numerical solutions for the SCIR model at selected time points, reflecting the dynamics of pneumococcal pneumonia under a fractional derivative formulation. The columns represent the populations of susceptible individuals ($S(t)$), carriers ($C(t)$), infected individuals ($I(t)$), and recovered individuals ($R(t)$) at different time points. The time t indicates the progression of the disease, showing how these populations evolve. The susceptible population $S(t)$ initially represents 90% of the population and decreases as individuals either become carriers ($C(t)$) or directly infected ($I(t)$), or die. The carrier population $C(t)$, starting at 15%, increases initially as more susceptible individuals transition to carriers but then decreases as they progress to infection, recovery, or death. The infected population $I(t)$, starting at 75%, decreases over time as individuals recover or die, indicating that the infection is being controlled. The recovered population $R(t)$, starting at 10%, increases over time, showing the growing number of individuals who recover. The system exhibits a decline in $S(t)$ and a rise in $R(t)$, with the peak of carriers and infected individuals occurring early, signaling an initial outbreak phase followed by stabilization. However, $S(t)$ does not reach zero, suggesting that a portion of the population remains susceptible, possibly leading to future outbreaks. The Caputo fractional derivative introduces memory effects, making the disease's progression slower and with a longer-lasting impact, as the rate of change in each compartment is influenced by past states. This results in a more gradual decline in infected individuals compared with classical models. The table captures the transient dynamics of pneumococcal pneumonia under this fractional formulation, demonstrating how the disease spreads, peaks, and declines, with past infections continuing to influence the present, leading to a slower decay of infections. Table 4: Numerical solutions for the populations $S(t)$, $C(t)$, $I(t)$, and $R(t)$ at selected time points, demonstrating the dynamics of pneumococcal pneumonia under the fractional derivative formulation.

Table 4. Numerical solutions for $S(t)$, $C(t)$, $I(t)$, and $R(t)$ at selected time points.

Time t	$S(t)$	$C(t)$	$I(t)$	$R(t)$
0.00	0.9000	0.1500	0.7500	0.1000
0.10	0.8233	0.1695	0.6781	0.1480
0.51	0.6526	0.1721	0.4473	0.2858
0.91	0.6018	0.1365	0.2996	0.3477
1.01	0.5982	0.1271	0.2715	0.3551
1.41	0.6042	0.0934	0.1845	0.3626
1.52	0.6098	0.0856	0.1663	0.3599
2.02	0.6460	0.0573	0.1051	0.3328
2.53	0.6913	0.0384	0.0674	0.2921
3.03	0.7362	0.0263	0.0446	0.2495
3.54	0.7788	0.0182	0.0299	0.2082

9. Numerical simulation

Figure 4: Comparison between the LAPM and ABM solutions for the susceptible population $S(t)$ under different fractional-orders.

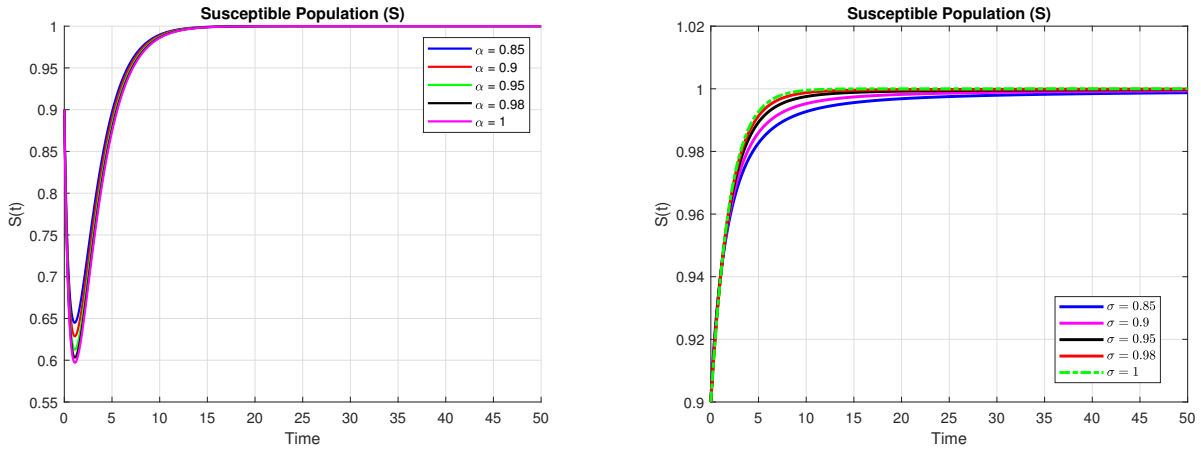

(a) Under the LAPM (b) Under the Caputo operator

Figure 4. A comparison between the LAPM and ABM for the susceptible population (S(t)) with different fractional-orders.

Figure 5: Comparison between the LAPM and ABM solutions for the carrier population $C(t)$ under different fractional-orders.

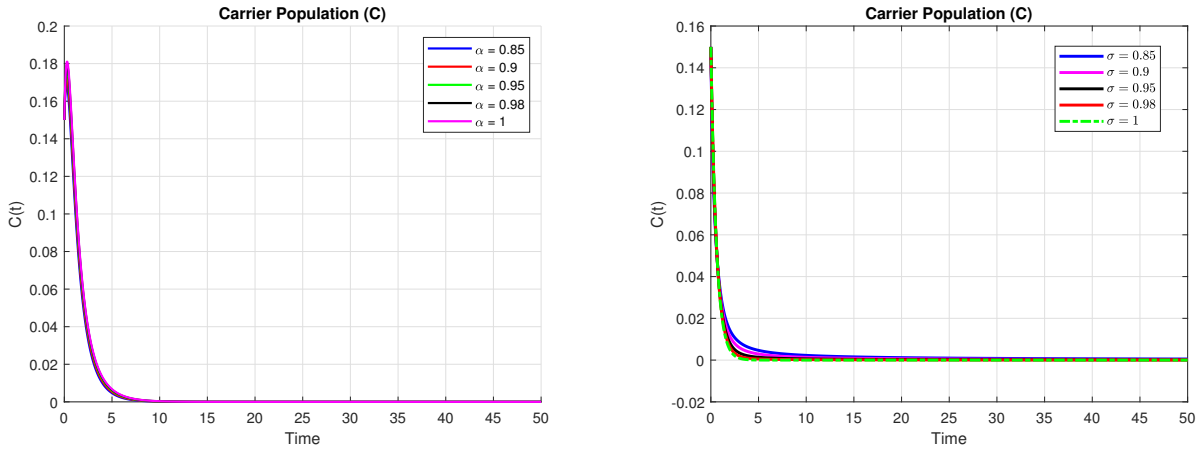

(a) Under the LAPM (b) Under the Caputo operator

Figure 5. A comparison between the LAPM and ABM for the carrier population (C(t)) with different fractional-orders.

Figure 6: Comparison between the LAPM and ABM solutions for the infected population $I(t)$ under different fractional-orders.

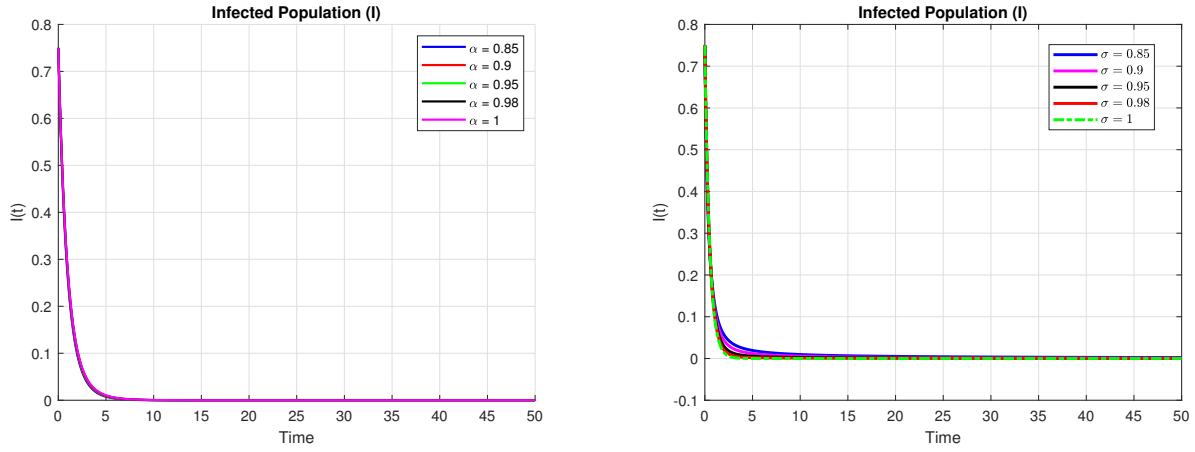

(a) Under the LAPM (b) Under the Caputo operator

Figure 6. A comparison between the LAPM and ABM for the infected population (I(t)) with different fractional-orders.

Figure 7: Comparison between the LAPM and ABM solutions for the recovered population $R(t)$ under different fractional-orders.

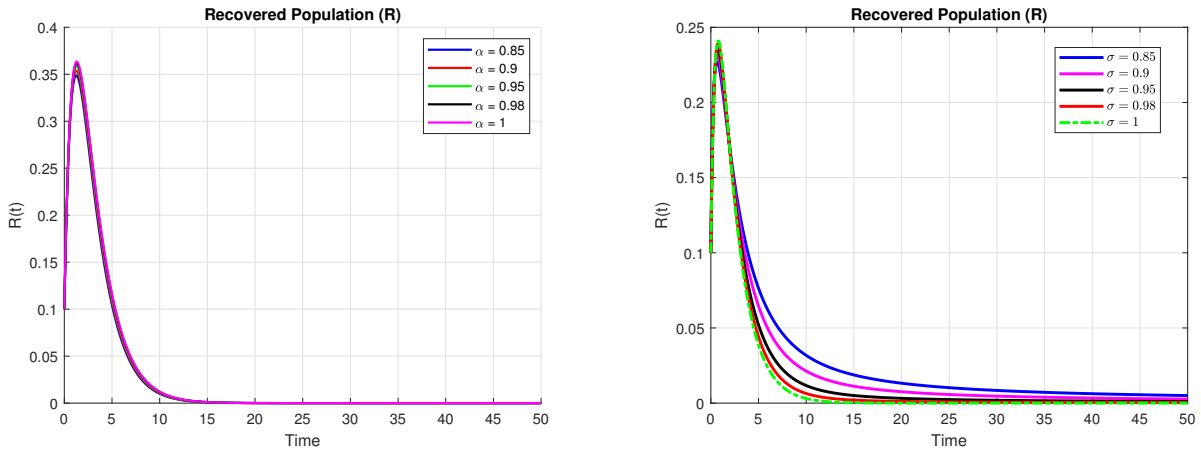

(a) Under the LAPM (b) Under the Caputo operator

Figure 7. A comparison between the LAPM and ABM for the recovered population (R(t)) with different fractional-orders.

Figure 8: Dynamics of the system (3.2) for $\rho = 1$ under both the LAPM and ABM, showing the evolution of susceptible, carrier, infected, and recovered populations over time.

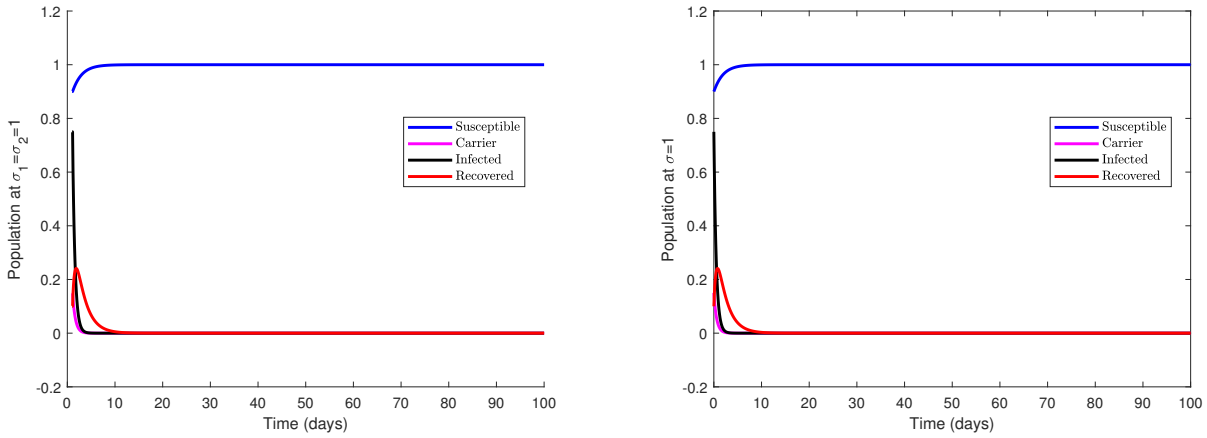

(a) Under the LAPM (b) Under the Caputo operator

Figure 8. Dynamics of the system (3.2) for $\varrho = 1$ under LAPM and ABM.

Figure 9: Dynamics of the system (3.2) for $\rho = 0.98$ under both the LAPM and ABM, showing the evolution of susceptible, carrier, infected, and recovered populations over time.

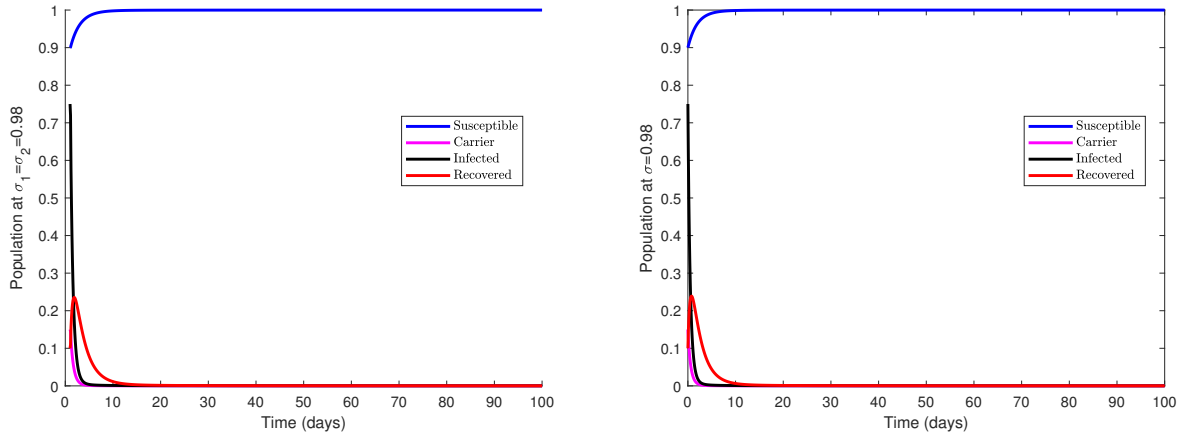

(a) Under the LAPM (b) Under the Caputo operator

Figure 9. Dynamics of the system (3.2) for $\varrho = 0.98$ under the LAPM and ABM.

Figure 10: Dynamics of the system (3.2) for $\rho = 0.95$ under both the LAPM and ABM.

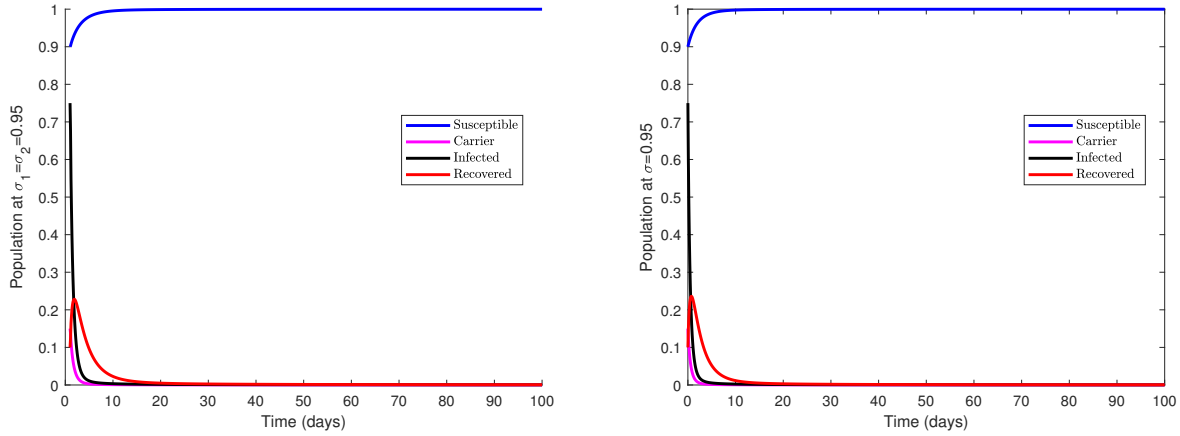

(a) Under the LAPM (b) Under the Caputo operator

Figure 10. Dynamics of the system (3.2) for $\varrho = 0.95$ under the LAPM and ABM.

Figure 11: Dynamics of the system (3.2) for $\rho = 0.90$ under both the LAPM and ABM.

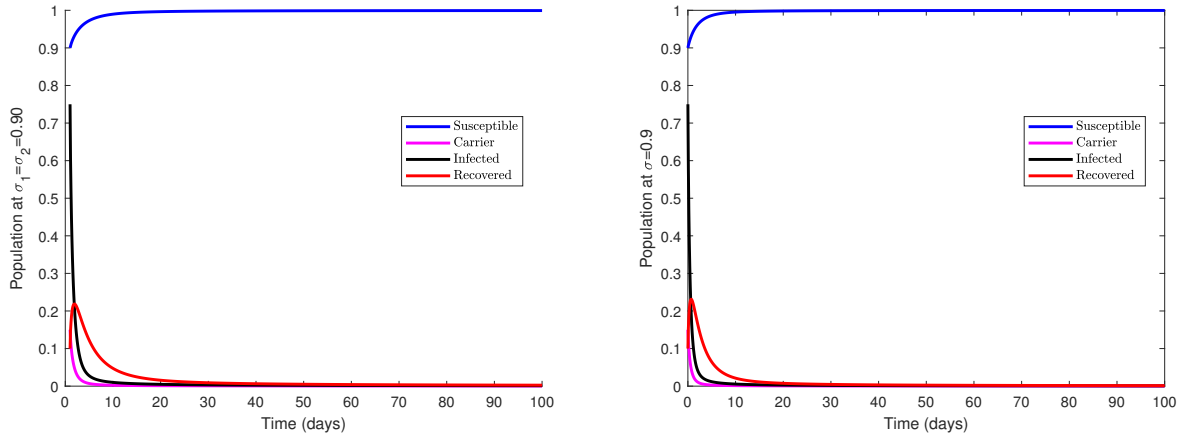

(a) Under the LAPM (b) Under the Caputo operator

Figure 11. Dynamics of the system (3.2) for $\varrho = 0.9$ under the LAPM and ABM.

Figure 12: Dynamics of the system (3.2) for $\rho = 0.85$ under both the LAPM and ABM.

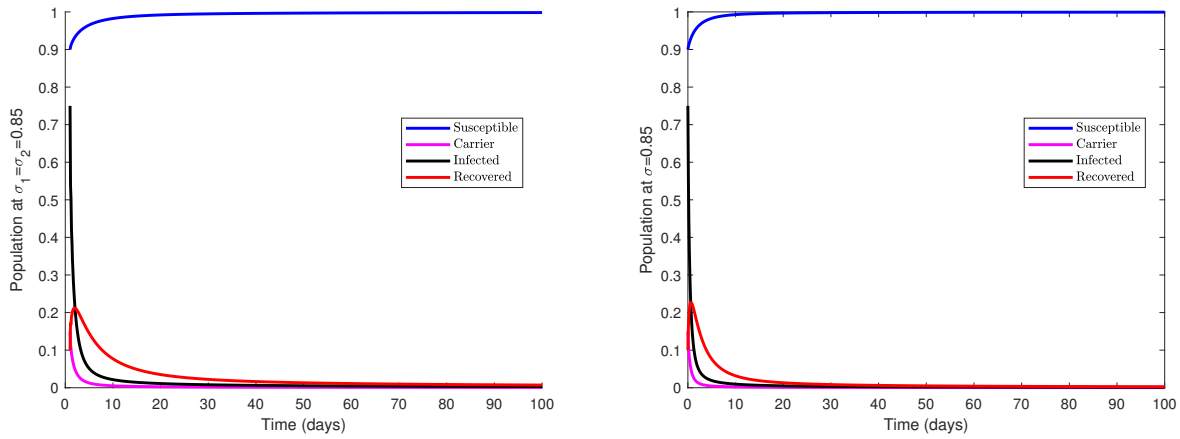

(a) Under the LAPM

(b) Under the Caputo operator

Figure 12. Dynamics of the system (3.2) for $\varrho = 0.85$ under the LAPM and ABM.

Table 5: Parameter values from AboDayeh, K. et al. [57], listing parameter symbols, descriptions, and their corresponding values used in the model simulations.

Table 5. Parameter values from AboDayeh, K. et al. [57].

Parameter	Description	Value
Π	Recruitment rate into the susceptible population	0.5
δ	Transmission rate	2 (DFE), 2.5 (EE)
Ω	Rate of vaccinated individuals	0.1124
μ	Natural mortality rate	0.5
η	Time when symptomatic infectious have symptoms	0.00641
–	Recovery rate of carriers	0.515
π	Rate of carriers developing symptoms	0.7096
θ	Proportion of susceptible individuals joining carriers	0.563
τ	Recovery rate for those infected with pneumonia	0.641
Φ	Disease-induced mortality rate	0.53

Figures 4–7 report the time evolution of the individual compartments across several fractional-orders $\varrho \in \{0.85, 0.90, 0.95, 0.98\}$ and the classical case $\varrho = 1$. Figure 4 shows the susceptible population $S(t)$, Figure 5 the carrier class $C(t)$, Figure 6 shows the infected class $I(t)$, and Figure 7 shows the recovered class $R(t)$. In all cases, fractional-order dynamics ($\varrho < 1$) slow the rates of change relative to the integer-order case, reflecting memory effects that alter the residence times and transition speeds.

In Figure 4, $S(t)$ decreases as individuals enter carriage or symptomatic infection; memory effects (smaller ϱ) slow this depletion by dampening the instantaneous response to the force of infection. Figure 5 shows $C(t)$ typically rising initially then declining as carriers progress to infection, recover, or die; fractional derivatives prolong the average residence time in carriage, delaying the

decline. Figure 6 displays the characteristic peak-decline outbreak profile of $I(t)$; relative to $\varrho = 1$, fractional-orders yield a flatter peak and a longer tail, indicating persistent low-level infection. Figure 7 shows $R(t)$ accumulating over time; memory affects effective recovery dynamics and the timing of returns to susceptibility (via waning), thereby modulating the reinfection risk.

A key advantage of fractional modeling is that each state depends on its full history, not only the instantaneous rates. To quantify this, we compare the trajectories for $\varrho \in \{0.85, 0.90, 0.95, 0.98\}$ against the classical case $\varrho = 1$. A decreasing ϱ (stronger memory) consistently (i) slows the decay of $I(t)$ and lengthens the persistence of $C(t)$, (ii) reduces peak prevalence in $I(t)$ but stretches it over a longer interval; and (iii) attenuates the initial decline in $S(t)$. For illustration, in our simulations, the infection prevalence falls below 5% of the population by Day 20 when $\varrho = 1$, whereas the same threshold is reached at approximately Day 28 for $\varrho = 0.90$ and Day 35 for $\varrho = 0.85$. These quantitative differences align with prolonged pneumococcal carriage, waning immunity, and reinfection risk-features inadequately represented by classical integer-order models.

Figures 8–12 display the joint evolution of (S, C, I, R) for $\varrho \in \{1, 0.98, 0.95, 0.90, 0.85\}$ under both the LAPM and ABM solvers. As ϱ decreases, the epidemic wave in $I(t)$ is flattened and delayed, the depletion of $S(t)$ is moderated, and the residence time in $C(t)$ increases, yielding longer epidemic tails and sustained carriage. The close agreement between the LAPM and ABM across these panels indicates that the observed trends are robust to the numerical scheme used.

9.1. Comparative discussion: The LAPM and ABM versus standard schemes

To assess the performance of our solvers, we contrast the LAPM and the fractional ABM predictor-corrector with two standard references: the L1 Caputo discretization on uniform/graded meshes (widely used finite-difference scheme) and spectral collocation (e.g., Jacobi/Chebyshev) as a high-accuracy benchmark for smooth problems.

Accuracy and convergence. Let $0 < \alpha < 1$ be the fractional order and h be the time step.

- L1 (Caputo). On uniform meshes, the L1 formula reaches up to $O(h^{2-\alpha})$ under suitable regularity; graded meshes (with grading exponent tuned to α) mitigate start-up singularities and improve early-time accuracy without excessive refinement.
- ABM. For ${}^{\mathrm{C}}D_t^{\alpha} y = f(t, y)$ under the standard Lipschitz/regularity conditions, the global error behaves like $O(h^{\min\{2,\, 1+\alpha\}})$—strictly higher than first-order for all $\alpha > 0$, approaching second-order as $\alpha \to 1$.
- LAPM (Adomian + Padé). For analytic right-hand sides, the Adomian series captures nonlocal memory while Padé resummation accelerates convergence, often delivering near-spectral accuracy up to the nearest complex singularity. In practice, modest truncation already matches or exceeds time-marching accuracy.

Stability and robustness. Implicit L1 improves damping along the negative real axis for the test equation ${}^{\mathrm{C}}D_t^{\alpha} y = \lambda y$ with $\Re(\lambda) < 0$ at the cost of a (non)linear solve per step. ABM's corrector provides robust long-time transients for the SCIR dynamics under standard step-size controls. LAPM's stability depends on series truncation and Padé degrees; with moderate orders, it is robust over our parameter ranges and avoids cumulative step-by-step amplification. Spectral collocation is stable for smooth

instances but can be sensitive to boundary layers or piecewise forcing unless domain decomposition or adapted bases are used.

Computational efficiency and memory. History-convolution solvers (L1, ABM) require the full past, yielding naïve $O(N^2)$ time and $O(N)$ memory over N steps; both benefit from fast-convolution/short-memory strategies that reduce the cost toward $O(N \log N)$ with $O(N)$ memory. ABM typically achieves a better accuracy-cost ratio at moderate h due to its predictor-corrector structure. LAPM front-loads the cost into generating a truncated series and Padé wrap; subsequent evaluation at many time points and parameter sets is inexpensive, which is advantageous for parameter sweeps and calibration. Spectral collocation shifts work to dense solves/transforms per time slab; efficient at moderate degrees, but less flexible under frequent parameter changes.

Implementation and flexibility. L1 remains simple and effective, with graded meshes recommended near $t = 0$. ABM strikes a favorable balance: IT is straightforward to code, compatible with adaptivity/graded meshes, and preserves positivity/invariant sets for the SCIR state under standard step-size restrictions. LAPM requires generating Adomian polynomials and selection of Padé orders, but once configured, it yields reference-quality trajectories with minimal runtime for scenario analysis. Spectral collocation is elegant for smooth kinetics yet demands careful basis/quadrature/filters for robustness in nonsmooth regimes.

Summary and recommendation for the SCIR model. LAPM provides high-fidelity reference solutions at a low computational cost and serves as our benchmark. ABM offers an excellent accuracy-efficiency trade-off for routine time-domain simulations and is our recommended workhorse (especially with graded meshes or fast-convolution acceleration). L1 remains a valuable baseline and cross-check, particularly when paired with mesh grading. Spectral collocation is best reserved for validation on smooth instances rather than large-scale or real-time runs.

Table 6: Qualitative comparison for $CD_\alpha ty = f(t, y), 0 < \alpha < 1$, summarizing the performance of different numerical methods (L1 Caputo, ABM, LAPM, and Spectral Collocation) based on their order, time & memory efficiency, robustness, and suitability for different problem types.

Table 6. Qualitative comparison for ${}^{\mathrm{C}}D_t^\alpha y = f(t, y), 0 < \alpha < 1$.

Method	Order	Time & memory	Robustness	Notes
L1 (Caputo)	Up to $O(h^{2-\alpha})$	$O(N^2)$ / $O(N)$	Good (implicit)	Graded mesh near $t = 0$ recommended.
ABM (PECE)	$O(h^{\min\{2,\,1+\alpha\}})$	$O(N^2)$; $\rightarrow$ $O(N \log N)$ with fast conv.	Robust	Workhorse for SCIR simulations.
LAPM (A+P)	Near-spectral (analytic RHS)	Offline series; cheap eval	Robust if degrees moderate	Benchmark / parameter sweeps.
Spectral collocation	Exponential (smooth)	Dense solves/transforms	Sensitive to nonsmooth	Best for validation on smooth cases.

10. Discussion

This work develops and analyzes a fractional-order SCIR framework for pneumococcal pneumonia that explicitly captures memory in transmission, carriage, recovery, and waning immunity. In contrast to classical, memoryless formulations, the fractional setting reproduces longer transients: peaks in symptomatic infection are flattened and delayed, depletion of the susceptible class is slower, residence in the carrier class is extended, and epidemic tails are longer. These patterns are consistent with the biology of pneumococcal disease, where prolonged asymptomatic carriage, partial and waning immunity, and reinfection are well documented.

Although SCIR models with fractional operators have appeared in related contexts, the present formulation is tailored to pneumococcal pneumonia and yields several new insights. First, we identify a clear threshold quantity that separates elimination from persistence and show that memory shifts this threshold relative to the classical setting. Second, we demonstrate solver-robust qualitative behavior by comparing two complementary computational approaches: the Laplace-Adomian-Padé method as a semi-analytical validator and the Adams-Bashforth-Moulton predictor-corrector as a practical time-marching scheme. Their agreement across scenarios supports the reliability of our findings and indicates that the observed effects are model-intrinsic rather than artifacts of a particular algorithm.

The sensitivity analysis clarifies intervention priorities. Reducing effective contacts and lowering carriage prevalence exert the strongest influence on transmission potential. Faster clinical removal improves individual outcomes and contributes to control, but its marginal impact on transmission is typically smaller than measures that limit contact or prevent colonization. These results translate into concrete guidance for public health practice: Combine sustained contact reduction with strategies that prevent acquisition and progression from carriage, while maintaining strong case management to reduce morbidity and mortality.

The classical SCIR model is recovered as a special case when memory is absent. Side-by-side simulations show that the classical model predicts shorter outbreaks and a faster return to equilibrium, whereas the fractional framework reproduces the extended behavior often observed in practice. This distinction matters for planning: Memory-aware models imply longer decision horizons and argue against short, one-off campaigns in favor of sustained, adaptive interventions.

This study focuses on qualitative behavior. For policy-ready use, parameter values should be anchored to epidemiological evidence, including natural mortality, average duration of carriage, progression from carriage to symptomatic infection, clinical recovery, and disease-induced mortality. Calibration against region-specific datasets would enable quantitative prediction and scenario testing. Additional realism can be introduced by incorporating age structure, spatial coupling, heterogeneity in contact patterns, and time-varying controls. Finally, coupling the model with uncertainty quantification and cost-effectiveness analysis would further strengthen its utility for decision makers.

11. Conclusions

We present a unified, memory-aware SCIR framework for pneumococcal pneumonia that establishes well-posedness, identifies and analyzes the governing threshold for elimination versus persistence, proves stability of both disease-free and endemic regimes, ranks epidemiological drivers through sensitivity analysis, and validates qualitative behavior with two complementary numerical

schemes. Collectively, the results show that accounting for memory yields slower, longer outbreaks and shifts control priorities toward sustained contact reduction and interventions that reduce carriage, with timely treatment remaining essential for limiting severe outcomes.

Practically, the findings support a balanced portfolio of measures: reduce opportunities for transmission, prevent or shorten carriage, and maintain effective case management. Because memory stretches epidemic transients, planners should anticipate delayed peaks and extended tails when sizing resources, timing vaccination, and evaluating time to elimination. Future work will integrate real data for calibration and validation, introduce demographic and spatial heterogeneity, explore alternative memory kernels and distributed orders, and develop an optimal-control and economic-evaluation layer to translate the model's thresholds into operational public-health strategies.

Author contributions

Muflih Alhazmi: Software validation, visualization, writing-review & editing. Safa M. Mirgani: Investigation, data curation, writing-review & editing. Abdullah Alahmari: Software validation, visualization, resource, funding acquisition. Sayed Saber: Conceptualization, methodology, formal analysis, writing-original draft, supervision. All authors have read and agreed to the published manuscript version.

Use of Generative-AI tools declaration

The authors declare that they have not used Artificial Intelligence (AI) tools in the creation of this article.

Funding

This work was supported and funded by the Deanship of Scientific Research at Imam Mohammad Ibn Saud Islamic University (IMSIU) (grant number IMSIU-DDRSP2501).

Conflict of interest

All authors declare no conflicts of interest in this paper.

References

1. O. J. Otieno, M. Joseph, O. Paul, Mathematical model for pneumonia dynamics with carriers, *Int. J. Math. Anal.*, **7** (2013), 2457–2473. https://doi.org/10.12988/ijma.2013.35109
2. E. Mochan, D. Swigon, G. B. Ermentrout, S. Lukens, G. Clermont, A mathematical model of intrahost pneumococcal pneumonia infection dynamics in murine strains, *J. Theor. Biol.*, **353** (2014), 44–54. https://doi.org/10.1016/j.jtbi.2014.02.021
3. G. L. Drusano, W. Liu, S. Fikes, R. Cirz, N. Robbins, S. Kurhanewicz, et al., Interaction of drug- and granulocyte-mediated killing of J. Pseudomonas aeruginosa in a murine pneumonia model, *J. Infect. Dis.*, **210** (2014), 1319–1324. https://doi.org/10.1093/infdis/jiu237

4. E. J. Ndelwa, M. Kgosimore, E. S. Massawe, L. Namkinga, Mathematical modelling and analysis of treatment and screening of pneumonia, *Math. Theor. Model.*, **5** (2015), 21–39.
5. K. Kosasih, U. R. Abeyratne, V. Swarnkar, R. Triasih, Wavelet augmented cough analysis for rapid childhood pneumonia diagnosis, *IEEE T. Biomed. Eng.*, **62** (2015), 1185–1194. https://doi.org/10.1109/TBME.2014.2381214
6. A. C. G. César, L. F. C. Nascimento, K. C. C. Mantovani, L. C. P. Vieira, Fine particulate matter estimated by mathematical model and hospitalisations for pneumonia and asthma in children, *Rev. Paul. Pediatr.*, **34** (2016), 18–23. https://doi.org/10.1016/j.rpped.2015.06.009
7. C. Marchello, A. P. Dale, T. N. Thai, D. S. Han, M. H. Ebell, Prevalence of atypical pathogens in patients with cough and community-acquired pneumonia: A meta-analysis, *Ann. Fam. Med.*, **14** (2016), 552–566. https://doi.org/10.1370/afm.1993
8. Y. H. Cheng, S. H. You, Y. J. Lin, S. C. Chen, W. Y. Chen, W. C. Chou, et al., Mathematical modeling of post coinfection with influenza A virus and Streptococcus pneumoniae, with implications for pneumonia and COPD-risk assessment, *Int. J. Chronic Obstr.*, **12** (2017), 1973–1988. https://doi.org/10.2147/COPD.S138295
9. K. Kosasih, U. Abeyratne, Exhaustive mathematical analysis of simple clinical measurements for childhood pneumonia diagnosis, *World J. Pediatr.*, **13** (2017), 446–456. https://doi.org/10.1007/s12519-017-0019-4
10. G. T. Tilahun, O. D. Makinde, D. Malonza, Modelling and optimal control of pneumonia disease with cost-effective strategies, *J. Biol. Dyn.*, **11** (2017), 400–426. https://doi.org/10.1080/17513758.2017.1337245
11. G. T. Tilahun, O. D. Makinde, D. Malonza, Co-dynamics of pneumonia and typhoid fever diseases with cost effective optimal control analysis, *Appl. Math. Comput.*, **316** (2018), 438–459. https://doi.org/10.1016/j.amc.2017.07.063
12. A. Y. Amrulloh, U. R. Abeyratne, V. Swarnkar, D. Herath, R. Triasih, A. Setyati, HMM based cough sound analysis for classifying pneumonia and asthma in pediatric population, In: *EMBEC & NBC 2017*, Singapore: Springer, 2018. https://doi.org/10.1007/978-981-10-5122-7_213
13. M. Kizito, J. Tumwiine, A mathematical model of treatment and vaccination interventions of pneumococcal pneumonia infection dynamics, *J. Appl. Math.*, **2018** (2018), 2539465. https://doi.org/10.1155/2018/2539465
14. F. K. Mbabazi, J. Y. T. Mugisha, M. Kimathi, Modeling the within-host coinfection of influenza A virus and pneumococcus, *Appl. Math. Comput.*, **339** (2018), 488–506. https://doi.org/10.1016/j.amc.2018.07.031
15. G. T. Tilahun, Optimal control analysis of pneumonia and meningitis coinfection, *Comput. Math. Method. M.*, **2019** (2019), 1–15. https://doi.org/10.1155/2019/2658971
16. I. M. Diah, N. Aziz, Stochastic modelling for pneumonia incidence: A conceptual framework, *AIP Conf. Proc.*, **2138** (2019), 050010. https://doi.org/10.1063/1.5121115
17. G. T. Tilahun, Modeling co-dynamics of pneumonia and meningitis diseases, *Adv. Differ. Equ.*, **2019** (2019), 149. https://doi.org/10.1186/s13662-019-2087-3
18. F. K. Mbabazi, J. Y. T. Mugisha, M. Kimathi, Analysis of pneumococcal pneumonia with time delays, *Abstr. Appl. Anal.*, **2019** (2019), 3757036. https://doi.org/10.1155/2019/3757036

19. D. Otoo, P. Opoku, S. Charles, A. P. Kingsley, Deterministic epidemic model for ($SVC_{Sy}C_{Asy}IR$) pneumonia dynamics, with vaccination and temporal immunity, *Infect. Dis. Model.*, **5** (2020), 42–60. https://doi.org/10.1016/j.idm.2019.11.001
20. O. C. Zephaniah, U. I. R. Nwaugonma, I. S. Chioma, O. Adrew, A mathematical model and analysis of an SVEIR model for Streptococcus pneumoniae with saturated incidence force of infection, *Math. Model. Appl.*, **5** (2020), 16. https://doi.org/10.11648/j.mma.20200501.13
21. S. Saber, A. Alahmari, Impact of fractal-fractional dynamics on pneumonia transmission modeling, *Eur. J. Pure Appl. Math.*, **18** (2025), 5901. https://doi.org/10.29020/nybg.ejpam.v18i2.5901
22. M. Althubyani, N. E. Taha, K. O. Taha, R. A. Alharb, S. Saber, Epidemiological modeling of pneumococcal pneumonia: Insights from ABC fractal-fractional derivatives, *Comput. Model. Eng. Sci.*, **143** (2025), 3491–3521. https://doi.org/10.32604/cmes.2025.061640
23. N. Almutairi, S. Saber, H. Ahmad, The fractal-fractional Atangana-Baleanu operator for pneumonia disease: stability, statistical and numerical analyses, *AIMS Math.*, **8** (2023), 29382–29410. https://doi.org/10.3934/math.20231504
24. M. Naveed, D. Baleanu, A. Raza, M. Rafiq, A. H. Soori, M. Mohsin, Modeling the transmission dynamics of delayed pneumonia-like diseases with a sensitivity of parameters, *Adv. Differ. Equ.*, **2021** (2021), 468. https://doi.org/10.1186/s13662-021-03618-z
25. Y. Guo, T. Li, Fractional-order modeling and optimal control of a new online game addiction model based on real data, *Commun. Nonlinear Sci. Numer. Simul.*, **121** (2023), 107221. https://doi.org/10.1016/j.cnsns.2023.107221
26. J. Cao, Y. Wang, A. Alofi, A. Al-Mazrooei, A. Elaiw, Global stability of an epidemic model with carrier state in heterogeneous networks, *IMA J. Appl. Math.*, **80** (2015), 1025–1048. https://doi.org/10.1093/imamat/hxu040
27. R. L. Bagley, R. A. Calico, Fractional order state equations for the control of viscoelastically damped structures, *J. Guid. Control Dynam.*, **14** (1991), 304–311.
28. D. Kusnezov, A. Bulgac, G. D. Dang, Quantum Lévy processes and fractional kinetics, *Phys. Rev. Lett.*, **82** (1999), 1136–1139. https://doi.org/10.1103/PhysRevLett.82.1136
29. K. I. A. Ahmed, D. S. Haroon, N. Almutairi, S. Saber, Analytical solutions for a class of variable-order fractional Liu system under time-dependent variable coefficients, *Results Phys.*, **56** (2024), 107311. https://doi.org/10.1016/j.rinp.2023.107311
30. M. Alhazmi, S. Saber, Glucose-insulin regulatory system: Chaos control and stability analysis via Atangana-Baleanu fractal-fractional derivatives, *Alex. Eng. J.*, **122** (2025), 77–90. https://doi.org/10.1016/j.aej.2025.02.066
31. M. Alhazmi, A. F. Aljohani, N. E. Taha, S. Abdel-Khalek, M. Bayram, S. Saber, Application of a fractal fractional operator to nonlinear glucose-insulin systems: Adomian decomposition solutions, *Comput. Biol. Med.*, **196** (2025), 110453. https://doi.org/10.1016/j.compbiomed.2025.110453
32. S. Saber, B. Dridi, A. Alahmari, M. Messaoudi, Hyers-Ulam stability and control of fractional glucose-insulin systems, *Eur. J. Pure Appl. Math.*, **18** (2025), 6152. https://doi.org/10.29020/nybg.ejpam.v18i2.6152
33. M. Althubyani, H. D. S. Adam, A. Alalyani, N. E. Taha, K. O. Taha, R. A. Alharbi, et al., Understanding zoonotic disease spread with a fractional order epidemic model, *Sci. Rep.*, **15** (2025), 13921. https://doi.org/10.1038/s41598-025-95943-6

34. E. Addai, L. Zhang, J. K. K. Asamoah, J. F. Essel, A fractional order age-specific smoke epidemic model, *Appl. Math. Model.*, **119** (2023), 99–118. https://doi.org/10.1016/j.apm.2023.02.019
35. S. Rezapour, H. A. Mohammadi, A study on the AH1N1/09 influenza transmission model with the fractional Caputo-Fabrizio derivative, *Adv. Differ. Equ.*, **2020** (2020), 488. https://doi.org/10.1186/s13662-020-02945-x
36. D. S. Haroon, M. Althubyani, S. M. Mirgani, S. Saber, An application of Newton's interpolation polynomials to the zoonotic disease transmission between humans and baboons system based on a time-fractal fractional derivative with a power-law kernel, *AIP Adv.*, **15** (2025), 045217. https://doi.org/10.1063/5.0253869
37. A. Alsulami, R. A. Alharbi, T. M. Albogami, N. H. E. Eljaneid, H. D. S. Adam, S. Saber, Controlled chaos of a fractal-fractional Newton-Leipnik system, *Thermal Sci.*, **28** (2024), 5153–5160. https://doi.org/10.2298/TSCI2406153A
38. T. Yan, M. Alhazmi, Y. Mukhtar, E. Amna, A. Abdulrahman, S. Saber, Analysis of a Lorenz model using Adomian decomposition and fractal-fractional operators, *Thermal Sci.*, **28** (2024), 5001–5009. https://doi.org/10.2298/TSCI2406001Y
39. M. Alhazmi, F. M. Dawalbait, A. Aljohani, K. O. Taha, H. D. S. Adam, S. Saber, Numerical approximation method and chaos for a chaotic system in sense of Caputo-Fabrizio operator, *Thermal Sci.*, **28** (2024), 5161–5168. https://doi.org/10.2298/TSCI2406161A
40. K. I. A. Ahmed, D. S. Haroon, M. Y. Youssif, S. Saber, Different strategies for diabetes by mathematical modeling: Applications of fractal-fractional derivatives in the sense of Atangana-Baleanu, *Results Phys.*, **52** (2023), 106892. https://doi.org/10.1016/j.rinp.2023.106892
41. K. I. A. Ahmed, S. M. Mirgani, A. Seadawy, S. Saber, A comprehensive investigation of fractional glucose-insulin dynamics: Existence, stability, and numerical comparisons using residual power series and generalized Runge-Kutta methods, *J. Taibah Univ. Sci.*, **19** (2025), 2460280. https://doi.org/10.1080/16583655.2025.2460280
42. K. I. A. Ahmed, D. S. Haroon, M. Y. Youssif, S. Saber, Different strategies for diabetes by mathematical modeling: Modified minimal model, *Alex. Eng. J.*, **80** (2023), 74–87. https://doi.org/10.1016/j.aej.2023.07.050
43. I. Ul Haq, N. Ali, A. Bariq, A. Akgul, D. Baleanu, M. Bayram, Mathematical modelling of COVID-19 outbreak using caputo fractional derivative: stability analysis, *Appl. Math. Sci. Eng.*, **32** (2024), 2326982. https://doi.org/10.1080/27690911.2024.2326982
44. R. E. Mickens, *Applications of nonstandard finite difference dchemes*, World Scientific, 2000. https://doi.org/10.1142/4272
45. Z. Eskandari, Z. Avazzadeh, R. Khoshsiar Ghaziani, B. Li, Dynamics and bifurcations of a discrete-time Lotka-Volterra model using nonstandard finite difference discretization method, *Math. Method. Appl. Sci.*, **48** (2025), 7197–7212. https://doi.org/10.1002/mma.8859
46. L. W. Roeger, Dynamically consistent discrete Lotka-Volterra competition models derived from nonstandard finite-difference schemes, *Discrete Contin. Dyn. Syst. B*, **9** (2008), 415–429. https://doi.org/10.3934/dcdsb.2008.9.415
47. K. K. Kataria, P. Vellaisamy, Saigo space-time fractional Poisson process via Adomian decomposition method, *Stat. Probab. Lett.*, **129** (2017), 69–80. https://doi.org/10.1016/j.spl.2017.05.007

48. F. Haq, K. Shah, G. ur Rahman, M. Shahzad, Numerical solution of fractional order smoking model via Laplace Adomian decomposition method, *Alex. Eng. J.*, **57** (2018), 1061–1069. https://doi.org/10.1016/j.aej.2017.02.015
49. S. Sirisubtawee, S. Kaewta, New modified Adomian decomposition recursion schemes for solving certain types of nonlinear fractional two-point boundary value problems, *Int. J. Math. Math. Sci.*, **2017** (2017), 5742965. https://doi.org/10.1155/2017/5742965
50. A. Freihat, S. Momani, Application of multistep generalized differential transform method for the solutions of the fractional-order Chua's system, *Discrete Dyn. Nat. Soc.*, **2012** (2012), 427393. https://doi.org/10.1155/2012/427393
51. M. H. Alshehri, F. Z. Duraihem, A. Alalyani, S. Saber, A Caputo (discretization) fractional-order model of glucose-insulin interaction: Numerical solution and comparisons with experimental data, *J. Taibah Univ. Sci.*, **15** (2021), 26–36. https://doi.org/10.1080/16583655.2021.1872197
52. H. Wang, D. Yang, S. Zhu, A Petrov-Galerkin finite element method for variable-coefficient fractional diffusion equations, *Comput. Method. Appl. M.*, **290** (2015), 45–56. https://doi.org/10.1016/j.cma.2015.02.027
53. J. Xie, Numerical computation of fractional partial differential equations with variable coefficients utilizing the modified fractional Legendre wavelets and error analysis, *Math. Method. Appl. Sci.*, **44** (2021), 7150–7164. https://doi.org/10.1002/mma.7252
54. H. Lu, P. W. Bates, W. Chen, M. Zhang, The spectral collocation method for efficiently solving PDEs with fractional Laplacian, *Adv. Comput. Math.*, **44** (2018), 861–878. https://doi.org/10.1007/s10444-017-9564-6
55. H. L. Li, L. Zhang, C. Hu, Y. Jiang, Z. Teng , Dynamical analysis of a fractional-order predator-prey model incorporating a prey refuge, *J. Appl. Math. Comput.*, **54** (2017), 435–449. https://doi.org/10.1007/s12190-016-1017-8
56. R. Magin, X. Feng, D. Baleanu, Solving the fractional order Bloch equation, *Concept. Magn. Reson. A*, **34** (2009), 16–23. https://doi.org/10.1002/cmr.a.20129
57. K. AboDayeh, A. Raza, M. Rafiq, M. S. Arif, M. Naveed, Z. Zeb, et al., Analysis of pneumonia model via efficient computing techniques, *Comput. Mater. Con.*, **70** (2022), 6073–6088. https://doi.org/10.32604/cmc.2022.020732
58. A. Boukhouima, K. Hattaf, N. Yousfi, Dynamics of a fractional order HIV infection model with specific functional response and cure rate, *Int. J. Differ. Equ.*, **2017** (2017), 8372140. https://doi.org/10.1155/2017/8372140
59. I. Podlubny, *Fractional differential equations*, Academic Press, 1998.

AIMS Press